The Pennsylvania State University

The Graduate School

College of Engineering

LOW-PH FE(II) OXIDATION USING A BIOREACTOR FOR THE TREATMENT OF ACID MINE DRAINAGE

A Thesis in

Environmental Engineering

by

Bradley Kaley

Submitted in Partial Fulfillment
of the Requirements
for the Degree of

Master of Science

December 2013

The thesis of Bradley Kaley was reviewed and approved* by the following:

William D. Burgos
Professor of Environmental Engineering
Thesis Advisor

John M. Regan
Professor of Environmental Engineering

Christopher A. Gorski
Assistant Professor in Civil Engineering

Peggy Johnson
Professor of Civil Engineering
Head of the Department of Civil and Environmental Engineering

*Signatures are on file in the Graduate School

ABSTRACT

This thesis examines the ability of a bioreactor to oxidize ferrous iron (Fe(II)) in acid mine drainage (AMD). An abandoned coal and clay mine near Dean, PA produces AMD at a site known as Brubaker Run, and this site was used in the study. Sediment and AMD were collected from Brubaker Run and used to enrich mixed-culture bioreactors in automated chemostats. The reactors were periodically dosed with ferrous sulfate to increase the Fe(II) concentrations. After the bioreactors were established, a series of flow-through experiments, with the reactors operating as completely-stirred tank reactors (CSTRs), were conducted to determine oxidation and removal rates at various operating conditions.

Two initial flow-through experiments were performed to determine an optimal hydraulic residence time. These tests were performed the same way, and from the calculated oxidation efficiencies for each hydraulic residence time tested, 6 h was chosen as the optimal value.

Using this hydraulic residence time, experiments were then conducted by varying the reactor pH and influent Fe(II) concentration of the bioreactors. Oxidation rates for these experiments increased with a decreasing reactor pH and with an increasing effluent Fe(II) concentration. Although the influent concentration was varied, the effects of the effluent concentration were examined because this is the concentration that was present in the bioreactor and available to the microorganisms. A saturation-like effect appeared to occur when the influent Fe(II) concentration reached the higher set points (1200 and 2400 mg/L). There was also a possible saturation-like effect from the hydrogen ion concentration when the reactor pH was decreased to 2.6 and 2.3.

From the experimental data, a general rate law model can be written for biological Fe(II) oxidation. Once simplified, it is only a function of the hydrogen ion and effluent Fe(II) concentrations. Measured pH and effluent Fe(II) values at the different operating conditions can be input into the simplified equation to predict the oxidation rates that should have been

measured. The model's predicted rates are not very accurate in terms of being similar to the actual measured rates. More experimental data or possibly even additional terms in the rate law equation are needed to produce a more accurate model.

The recorded addition of acid and base during the experiments can be used to show whether mainly Fe(II) oxidation or both Fe(II) oxidation and Fe(III) precipitation are occurring in the bioreactor. The data show evidence that at pH < 2.9 there is mainly Fe(II) oxidation occurring, while at pH > 2.9 both Fe(II) oxidation and Fe(III) precipitation are occurring. pH=2.9 needs to be explored more because the data do not show evidence for the occurrence of only oxidation or both oxidation and precipitation. The operating conditions are important because of the resulting reactions that they cause, and these reactions can be critical to the success of a treatment system.

The loading rates per area of the reactor (GDM) were found to be in the range of 9-448 g Fe(T)/d/m^2 (Fe(T)=total iron), depending on the operating conditions. Although this is a large range, the majority of the GDM values were above 60 g Fe(T)/d/m^2, and many were even above 100 g Fe(T)/d/m^2. The measured bioreactor GDM values were much larger than those reported in the literature. Thus, bioreactors appear to be a sensible choice for removing total iron from AMD.

TABLE OF CONTENTS

LIST OF FIGURES

LIST OF TABLES

ACKNOWLEDGEMENTS

I would like to first thank my thesis adviser, Bill Burgos, for all of his help and support throughout my research. Without his guidance this work would not have been possible. He has been a great adviser and I have enjoyed working for him.

I am also greatly appreciative off all of the other people in the department that have helped me along the way. From checking on my reactor when I was away to helping me transport site water from the Brubaker Run to the lab, someone was always willing to help. In particular, I'd like to thank Lance for providing support throughout the entire duration of my research. He has been there to help with anything I need.

I'd like to next thank my family for their support. They have always been there for me, with support and encouragement during both the good and frustrating times. I am thankful for everything they've done and continue to do.

Finally, I'd like to thank the Appalachian Research Initiative for Environmental Science for funding my work.

Chapter 1

Introduction

History and Impacts of Coal Mining

Mining activities, especially coal mining, have greatly increased since the start of the Industrial Revolution.[11] Much of the progress of industrialized nations would not have been possible without the products of the mining industry.[21] The constantly growing human population continues to require more of these mining products, and so there appears to be no end in sight for mining.[11]

While mining activities greatly benefit society, they also are a detriment.[21] Harvesting these natural resources can actually simultaneously contaminate other resources such as air, water, and soil.[21] As is especially true with surface mining, large areas of land and sometimes even entire sides of mountains can be removed in order to extract certain minerals. Contaminated water runoff from inside or on top of mines is also a problem because it eventually combines with other natural water systems.[11] With these problems occurring at both current and abandoned mining sites, the environmental impacts of mining need to be addressed to prevent further damage.

This thesis will focus only on the impacts of coal mining on water in Pennsylvania. Known for its extensive coal mining activities, Pennsylvania has at least 140 abandoned coal mines that are scattered throughout its bituminous and anthracite coal regions.[5] The locations of these mines are shown in Figure 1-1. The environmental impact of an abandoned mine is dependent on its condition at the time of abandonment, and if the mine is not properly sealed it will fill with water that will eventually be released when it reaches a certain level.[11] The sources

of the water filling the mine are groundwater and infiltration of surface water, both of which frequently or even continuously occur.[13] A series of reactions occur between the water and exposed rock within the mine, and the resulting contaminated water is known as acid mine drainage (AMD).[11] The geochemistry of AMD formation is discussed in the next section.

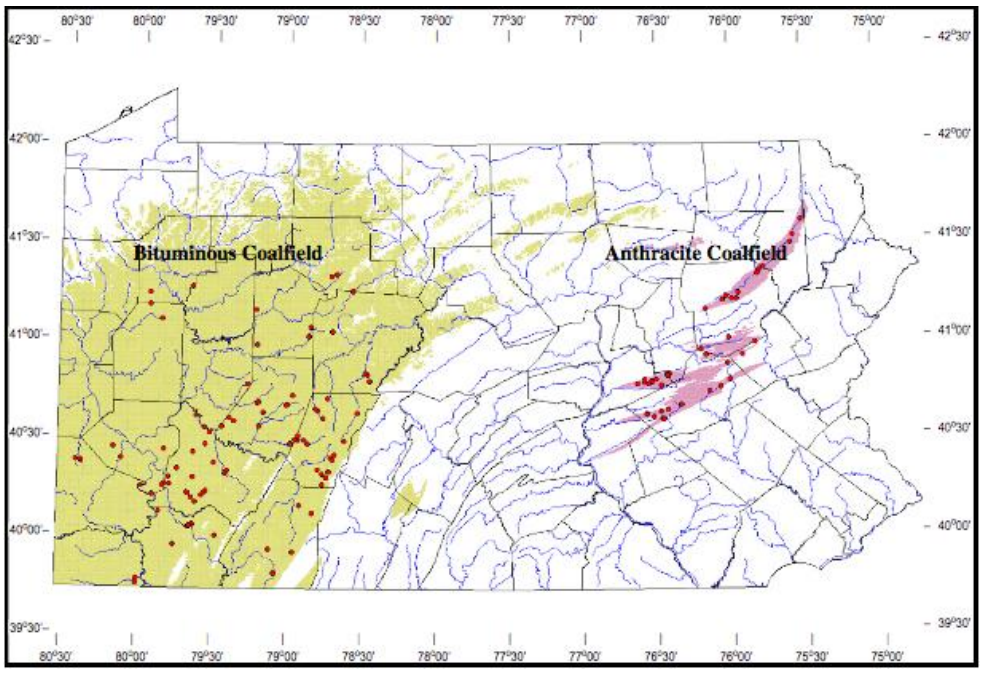

Figure 1-1: The red dots show the locations of abandoned coalmines in the two coal regions of Pennsylvania.[5]

Once released from a mine, AMD naturally combines with streams and rivers. Figure 1-2 shows the AMD-impacted streams in Pennsylvania and other Mid-Atlantic states. These impacted streams have little to no aquatic life because of the AMD.[3,21,22,26] Figure 1-3 shows a photo of the Red Moshannon, an AMD -impacted stream in Centre County, Pennsylvania. The large amount of iron precipitates have coated the streambed and turned it orange.

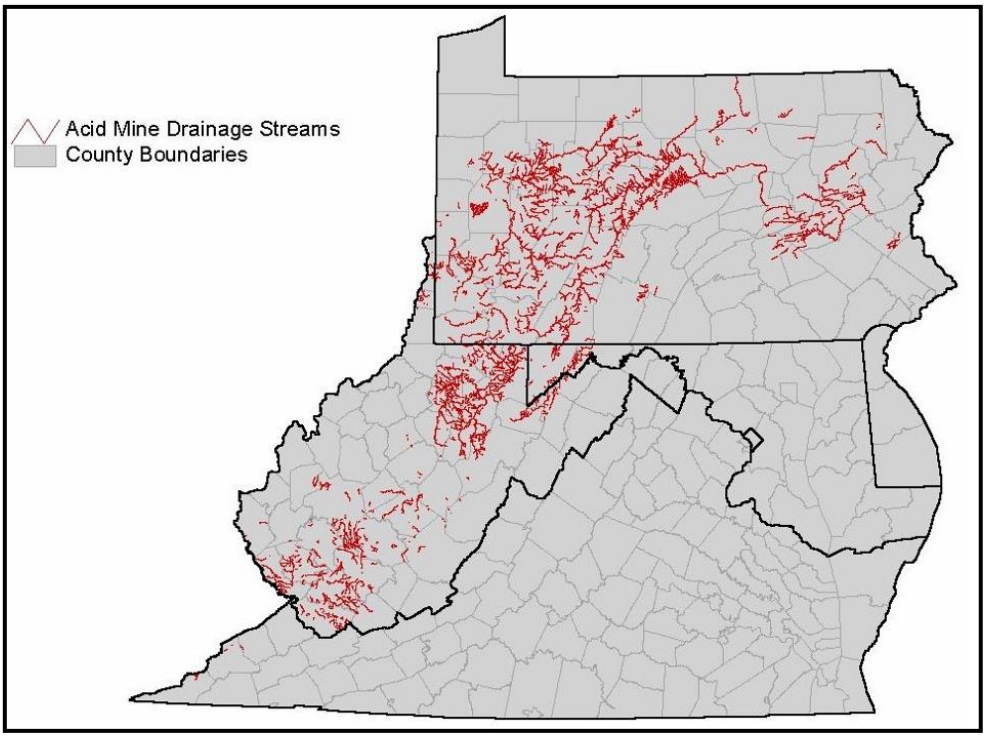

Figure 1-2: The streams affected by AMD are located in areas where abandoned coal mines are prevalent. (http://www.ei.lehigh.edu/envirosci/enviroissue/amd/links/graphs.html, accessed 10/30/2013)

Figure 1-3: The Red Moshannon in Pennsylvania is coated with an orange iron precipitate.

Geochemistry of AMD Formation

As stated previously, after a mine is abandoned it begins filling up with water if it is not properly sealed. The oxidative dissolution of sulfide compounds, one of which is pyrite, in the presence of oxygen and water causes AMD to form.[11,22] Other sulfide compounds can be the source of AMD formation, but in coalmines the main cause is pyrite.[26]

The four reactions shown below govern the formation of AMD in abandoned coalmines.[26]

$$FeS_2(s) + \frac{7}{2}O_2 + H_2O \leftrightarrow Fe^{2+} + 2SO_4^{2-} + 2H^+ \quad \text{(Reaction 1)}$$

$$Fe^{2+} + \frac{1}{4}O_2 + H^+ \leftrightarrow Fe^{3+} + \frac{1}{2}H_2O \quad \text{(Reaction 2)}$$

$$FeS_2(s) + 14Fe^{3+} + 8H_2O \leftrightarrow 15Fe^{2+} + 2SO_4^{2-} + 16H^+ \quad \text{(Reaction 3)}$$

$$Fe^{3+} + 3H_2O \leftrightarrow Fe(OH)_3 + 3H^+ \quad \text{(Reaction 4)}$$

Reaction 1 oxidizes the solid pyrite to produce soluble ferrous iron (Fe(II)) and acid (H^+), while Reaction 2 consumes acidity and oxidizes Fe(II) to ferric iron (Fe(III)). Fe(III) is then consumed in either the anaerobic oxidation of more pyrite (Reaction 3), or in the precipitation of ferrihydrite. Both Reactions 3 and 4 produce additional acidity.

In addition to the iron that is already present, other metals enter solution when they come in contact with low-pH AMD.[5] The hydrogen ions (H^+) that are produced in the above reactions cause dissolution of metal containing compounds when the AMD comes in contact with them.[5] The main constituents present are aluminum (Al), manganese (Mn), and sulfate (SO_4^{2-}).[5,11,26] It is important to note that although this discussion focuses on low-pH AMD, even higher pHs of 6-12 can actually be present.[11,22,26] In those cases, the acidity is due mineral acidity, which refers to the potential protons released after hydrolysis of metals as in Reaction 4.[26]

AMD Remediation

The remediation of AMD in general can be difficult because of the complex and varying geochemistries at different sites. The overall goals are to precipitate the metals and increase the pH if necessary.[12] If the remediation is focused simply on low-pH AMD containing high levels of iron, the approach is more direct. With these systems, the Fe(II) needs to be oxidized to Fe(III), which then needs to be precipitated as ferrihydrite or another ferric-hydroxide complex.[12] Reactions 2 and 4 from the previous section summarize these two processes. Precipitation of Fe(III) is achieved by increasing the pH to about 3.5.[26] Two approaches, passive and active, can be taken to accomplish these goals, and they are discussed in the following two sections.

Passive Treatment

A passive treatment system utilizes different treatment strategies depending on the geochemistry of the AMD, but all systems are typically built and then operated with little or no maintenance for many years.[7] These systems are both biological and abiotic in nature: they utilize microorganisms and aeration to oxidize iron and other metals, while limestone is used raise the pH.[7,12] Figure 1-4 shows a schematic of an ideal passive system. In this idealized figure, limestone is used to raise the pH. The series of ponds are used to oxidize, precipitate, and settle the iron before discharging the treated water.

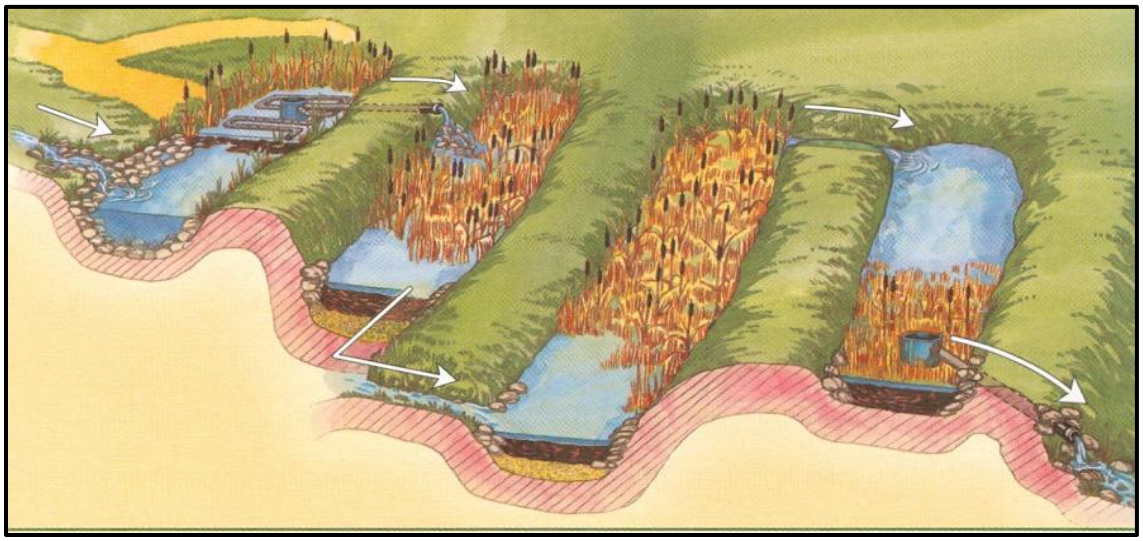

Figure 1-4: A passive treatment system is a sequence of ponds that treat the AMD with little or no maintenance required.[30]

These systems have pros and cons that need to be considered. Passive systems require little or no maintenance over most of their lifetime and are cheaper than active systems.[7,12] However, these systems are more susceptible to failure because of no daily maintenance and extreme weather conditions, which means they might not meet effluent standards.[7] Passive systems also have a large footprint because of the space required for the series of ponds.[12] More research is needed to perfect these systems and mitigate the problems that might deter engineers from selecting them.

Active Treatment

Contrary to passive systems that have little or no operation and maintenance, active systems require constant power to treat AMD.[12] Active systems abiotically treat AMD through aeration and alkaline chemical addition to oxidize iron and other metals and raise the pH.[12] The chemical addition can be done using one or more automated silos, as shown in Figure 1-5. After

aeration and chemical addition, the iron precipitates and requires a settling pond, or in some cases an engineered clarifier, to be removed.[12]

Figure 1-5: Silos can be used to raise the pH of AMD by actively dosing it with alkaline chemicals. (http://www.epa.gov/nrmrl/lrpcd/etsc/basic.html, accessed 10/30/2013).

There are advantages and disadvantages to active systems, just as there are for passive systems. Two obvious advantages are the ability to have operational control over the overall treatment processes, and a smaller required land area since large ponds are not needed. However, active systems are unfavorable because of the high cost of operation and maintenance, which includes costs for power and chemicals, some of which can be potentially hazardous.[7,12] These systems also produce large sludge volumes that need to be properly discarded.[12] Ideally, a combined active-passive system that utilizes both biological and abiotic strategies would be used in order to avoid some of the disadvantages.

Importance of Biological Fe(II) Oxidation at Low pH

In the previous section it was stated that the remediation strategy for iron removal from AMD is to oxidize all of the Fe(II) to Fe(III) so that it can precipitate and settle.[15,24] The pH of the water is very important because oxidation rates have been modeled with a dependency on

$[H^+]$.[15,23] Figure 1-6 shows this model, which includes both biological and abiotic Fe(II) oxidation. While the abiotic oxidation rate is very slow at pH < 4.5, above this pH the rate increases and is abiotically controlled.[15] This increasing abiotic rate is due to the strong pH dependency that is described in Equation 1-1,

$$\text{Rate}_{\text{abiotic}} = \frac{-k_{\text{abiotic}}[Fe^{2+}][O_2]}{[H^+]^2} \qquad (\text{Eq. } 1-1)$$

where $R_{abiotic}$ is the abiotic Fe(II) oxidation rate in (mol/L/s), $k_{abiotic}$ is the abiotic rate constant in (mol/L/s), $[Fe^{2+}]$ is the concentration of Fe(II) in (mol/L), $[O_2]$ is the concentration of dissolved oxygen in (mol/L), and $[H^+]$ is the concentration of hydrogen ions in (mol/L).[15] At pH < 4.5, where abiotic oxidation rates are very slow, the biological rate dominates.[15] The biological rate increases because of the pH dependency below pH=4.5, as described in Equation 1-2,

$$\text{Rate}_{\text{biological}} = -k_{\text{bio}} C_{\text{bacteria}} [Fe^{2+}] p_{O_2} [H^+] \qquad (\text{Eq. } 1-2)$$

where $R_{biological}$ is the biological Fe(II) oxidation rate in (mol/L/s), k_{bio} is the biological rate constant in (L^2/mg/mol/atm/s), $C_{bacteria}$ is the concentration of bacteria in (mg dry weight/L), and p_{O_2} is the partial pressure of oxygen in (atm).[15,23]

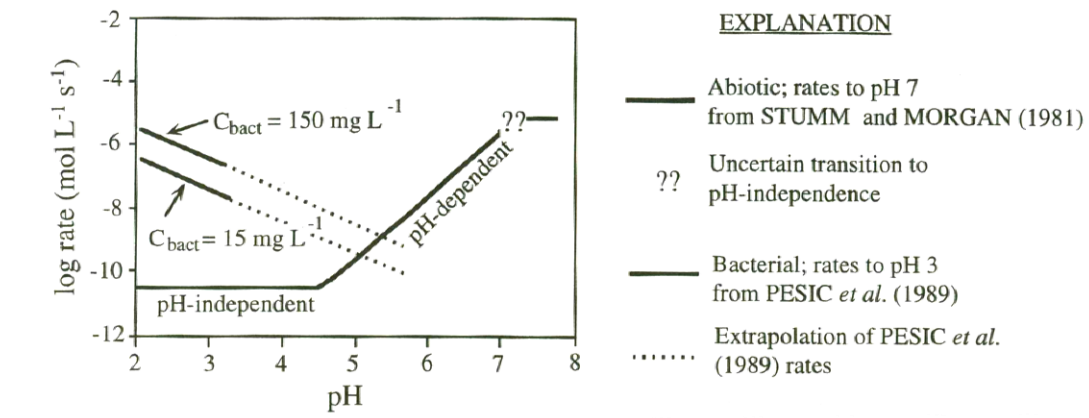

Figure 1-6: Plotted biological and abiotic rate equations show that a pH dependency exists.[12]

The biological low-pH portion of the previous model can be verified using measured oxidation rates in the literature. Figure 1-7 shows these measured rates plotted along with the abiotic model as a function of pH. Although these biological rates show a downward trend similar to the model in Figure 1-6, there are multiple orders of magnitude of variability between the values. Since the design of a low-pH biological Fe(II) treatment system is limited by these rates, it is important that they be studied more to lessen their variability.

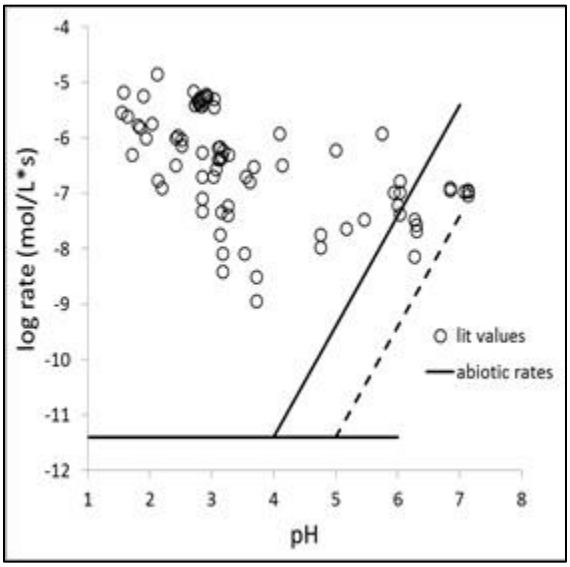

Figure 1-7: Compiled oxidation rates from the literature have been overlaid on the abiotic portion of the model from Figure 1-6.[2,14,27,29]

Current Natural Treatment by Terraced Iron Formations

Biological low-pH Fe(II) oxidation currently occurs naturally at some AMD sites.[1] Once the AMD emerges and is open to the atmosphere, the oxidation and precipitation of Fe(II) and Fe(III), respectively, begins as the AMD flows across the land.[11,26] Along the length of flow, iron precipitation can form terraced iron formations (TIFs) as shown in Figure 1-8.[1] Microorganisms are present on the TIFs and continuously oxidize the Fe(II).[1]

Figure 1-8: The upstream view of the Upper Red Eyes site in Pennsylvania shows the natural TIFs.

TIFs oxidize, precipitate, and remove iron from solution,[1] which is one of the goals of the treatment systems discussed previously. Although the TIFs destroy the area in which they are present, they are in fact a natural treatment process; therefore, utilizing their treatment capacity is only logical. The reported field oxidation rates are highly variable at low pHs, though, as was shown in Figure 1-7. Therefore, before TIFs can be utilized, the range of rates needs to be narrowed.

TIFs have the potential to be utilized in both passive and active treatment systems. They could serve as a pretreatment to the passive treatment system shown in Figure 1-4, or they might even replace the first and second ponds entirely. In an active system, they could be reconfigured into a bioreactor. In that case, the microorganisms that inhabit the TIFs would need to be transferred into the bioreactor. The traditional structure of the TIF would be compromised, but AMD flowing through the bioreactor would simulate flow across a TIF; therefore, biological Fe(II) oxidation would hopefully occur.

Studies on Low-pH Fe(II) Oxidation

Many studies have utilized low-pH Fe(II) oxidation in reactors. This research is important because they use different influent and reactor conditions to test the capacity of bioreactors for treatment. One important research setup is shown in Figure 1-9, and it utilized the iron oxidizer *Ferrovum myxofaciens*.[8] These bacteria were grown from a pure culture, and the feed water for the reactors was synthetic AMD.[8] The first reactor biologically oxidized Fe(II) to Fe(III), which subsequently precipitated and settled in the second reactor.[8] The pH in the second reactor was maintained at pH=3.5 in order to have optimal precipation.[8] The final reactor was a packed-bed bioreactor that removed any remaining Fe(II) and Fe(III).[8]

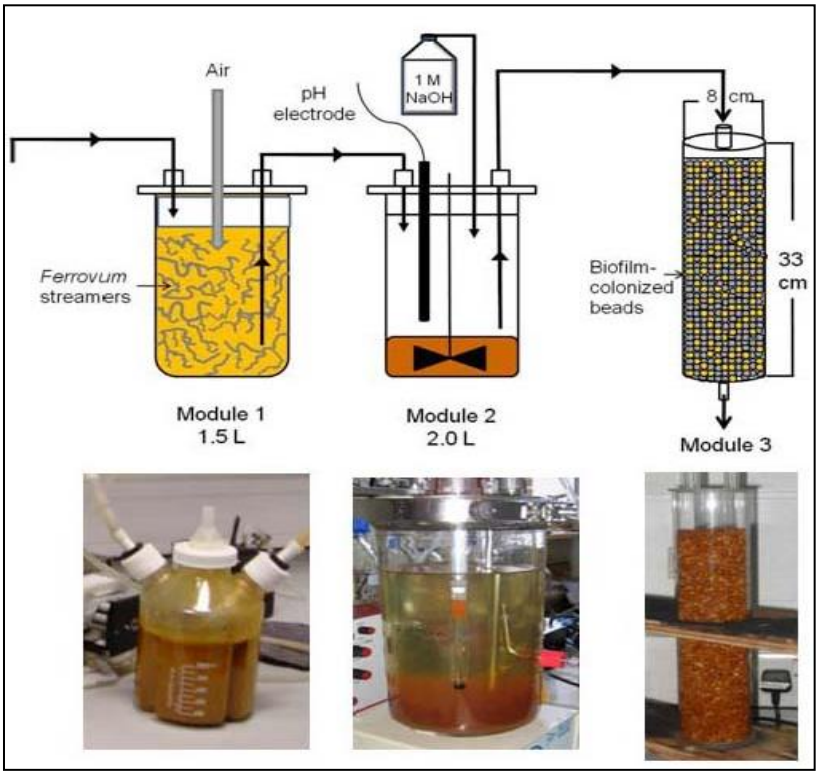

Figure 1-9: A three reactor system for low-pH iron oxidation and precipitation.[8,19]

This study tested different operational parameters for the first reactor and measured iron oxidation rates.[8] Varying flow rates (0.285 mL/h-810 mL/h), influent pHs (1.9-2.2, which corresponded to effluent pHs ranging from ~2.0-2.45), and influent Fe(II) concentrations (1-10

mM) were tested. Concentrations of sulfate, aluminum, manganese, copper, and zinc were also varied.[8] All operating conditions had little effect on iron oxidation rates in the reactor, except for the varying flow rates and influent Fe(II) concentrations. A lower flow rate increased the total percentage of Fe(II) oxidized, while increasing the concentration of influent Fe(II) caused a decrease in the percentage of Fe(II) oxidized. The results found in these experiments are important, but given the large range of pHs and Fe(II) concentrations found in AMD at different sites, the testing of a larger range of values for both of these parameters would be valuable.

Another experiment utilizing a bioreactor configuration was completed in a pilot plant treating AMD in Germany.[12] The pilot plant, pictured in Figure 1-10, consists of aeration, oxidation, and precipitation basins in series. The oxidation basin consists of large flat board-shaped materials that are suspended in the basin and provide a surface for the growth of microorganisms. Although this pilot plant focuses on collecting schwertmannite after the oxidation and precipitation of Fe(II) and Fe(III), respectively, it demonstrates the success, at least at the pilot scale level, of engineering a flow-through bioreactor to for low-pH Fe(II) oxidation.

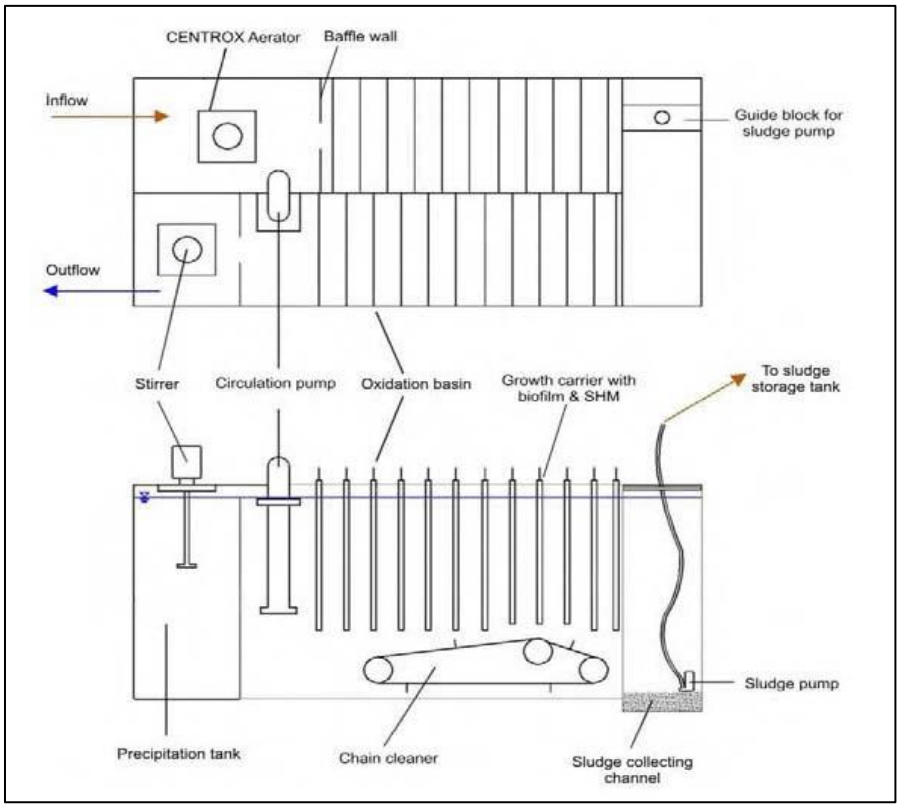

Figure 1-10: A pilot plant oxidizes Fe(II) biologically through the use of a biofilm present on materials submerged within the oxidation basin.[10]

Other studies have varied other operational parameters in a variety of reactor setups, and from these studies certain ranges of these operational parameters have been found to have no effect on Fe(II) oxidation rates. For pH, no effect on oxidation rates were found when it was varied from 2.00-3.25 in batch reactors,[6] from 1.5-2.5 in rotating biological contactors (RBCs),[18] or from 1.3-2.2 in an inverse fluidized bed bioreactor.[13]

Dissolved oxygen concentrations were found to have no effect as long as they were above 2 mg/L[6] or 0.64 mg/L.[20] Temperature was found to have no effect on rates when above 25°C in inverse fluidized bed bioreactors[13] or batch reactors,[6] or when in the range of 10-35°C in RBCs.[18] Finally, additional carbon dioxide bubbled into batch reactors was found not to affect oxidation rates.[6]

Research Objectives

Given the natural low-pH Fe(II) oxidation that occurs at AMD sites, there exists a great potential of utilizing this process. Although different operational parameters have been tested, some of the ranges of values tested have been narrow; therefore, a systematic variation of different parameters, specifically the reactor pH and influent Fe(II) concentration, must be performed. Also, past experiments, such as the one discussed in the previous section, used pure cultures. The more practical method for this would be to grow the bioreactor using native sediment and water from an AMD site. Data from experiments varying conditions in the bioreactor are important because they allow kinetic analyses to be employed to better understand the system. This increased understanding will improve potential designs if this bioreactor is ever implemented as part of a treatment system.

Based on these past studies, this work aimed to vary the hydraulic residence time, reactor pH, and influent Fe(II) concentration in a flow-through bioreactor containing a mixed culture of microorganisms collected from an AMD site. Overall, this research intends to answer the following questions:

1. What is the feasibility of enriching a mixed culture of iron oxidizers from sediment collected from an AMD site?
2. How does the oxidation rate within an established bioreactor change with varying hydraulic residence times (0.5-24 h), and what is the optimal value for this parameter?
3. How do the oxidation and precipitation rates in the bioreactor change with varying reactor pHs (2.3-4.1) and influent Fe(II) concentrations (80-2400 mg/L)?
4. How does the biomass concentration respond, in terms of its overall number and its distribution between the biofilm and suspension, to varying pHs and influent Fe(II) concentrations. Do these biomass concentrations affect the oxidation rates?

5. Can a general rate law be simplified and transformed into a model using data from these experiments, and then this model be used to accurately predict the oxidation rates that were achieved during the experiments?
6. Can the acid and base additions to the bioreactor throughout the experiments be used to help predict the predominant reactions occurring?
7. What are total iron removal rates in terms of loading rates per area of the bioreactor (GDM: grams of total iron per day per square meter) and how do they compare to other reported values?

Chapter 2

Methodology

Experimental Components

Field site and samples

The AMD site used in this study is known as Brubaker Run and is located in Dean, PA (40° 37'1.42" N, 78° 28'35.76" W). The reason for choosing Brubaker Run is that is exhibits similar Fe(II) oxidation field rates compared to other AMD sites in Pennsylvania and West Virginia.[16] At the site, AMD emerges from the abandoned coal and clay mine that used to be the location of both surface and underground mining.[3] The contaminated water emerges from two locations, one on the top of the hill and the other, known as BR-80, approximately halfway down the hill. The AMD from both emergences flows into Brubaker Run, which eventually combines with Clearfield Creek.[3] Severe degradation of aquatic life in Clearfield Creek is visible for up to 12 miles downstream of where Brubaker Run enters.[3] Currently there are no treatment systems in place at this site.

Sediment samples

Sediment samples were taken from the bottom of a pool, shown in Figure 2-1, located near the bottom of the TIF at Brubaker Run. Collected sediment was soft and easily removed from approximately the top 2-3 centimeters. These samples were transported to the lab in clean plastic containers and stored in the 4 ºC refrigerator for no longer than one week before use.

Figure 2-1: Sediment samples were taken from the bottom of this pool at Brubaker Run.

Water samples

Water samples were collected from the BR-80 emergence at Brubaker Run. The water emerging from the mine at this location is almost completely anoxic.[16] At BR-80, which is shown in Figure 2-2, the iron present in the water is almost entirely Fe(II), with a small fraction of Fe(III) present. This water was ideal because it provided a large consumable Fe(II) concentration for the microorganisms in the bioreactor.

Figure 2-2: Water samples were collected from the BR-80 mine emergence.

Polypropylene carboys ranging in size from 12-40 L were used to transport the water to the lab. Within 12 hours of the initial collection, samples were filtered using 0.2 micron Nalgene® bottle-top filters. This removed any suspended microorganisms and any other unwanted materials, such as leaves, grass, or iron solids. By removing the microorganisms from the water, little or no Fe(II) oxidation occurred, preserving the high Fe(II) to Fe(III) ratio. After being filtered, carboys containing the water were wrapped in aluminum foil or covered in cardboard boxes, and stored in the 4ºC refrigerator until use. The aluminum foil and cardboard boxes prevented light from entering the carboys and carrying out any possible photooxidation of the ferrous iron.

Reactors and Automated Control Units

Two Eppendorf BioFlo®/Celligen® 115 Fermentor/Bioreactor units were used for the experiments. One of the units is shown in Figure 2-3. Each collective unit is made of a reactor (chemostat) that is paired with its own automated control unit. The units can control pH, dissolved oxygen, agitation, and temperature. Three peristaltic pumps and an air sparger with manual flow rate control are also equipped on each unit. The units are connected to a computer that data logs all of the measurements taken by the control units at user-specified time intervals.

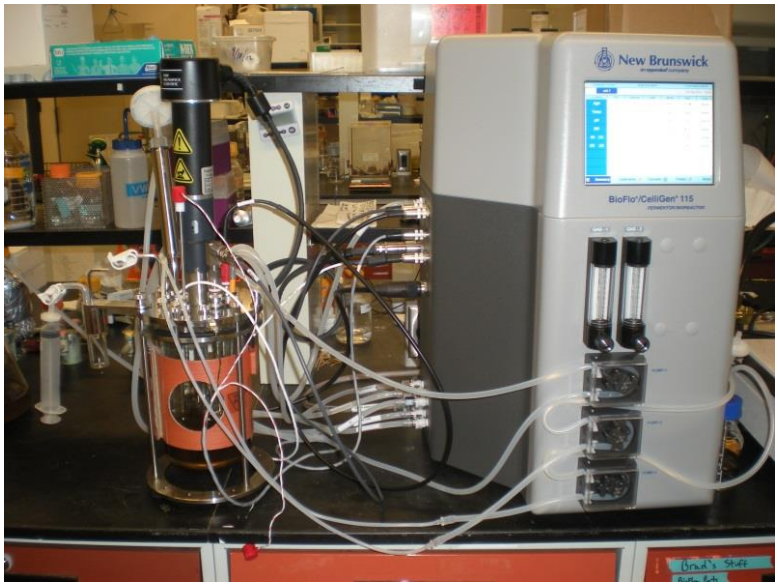

Figure 2-3: The automated control unit on the right regulates all of the operating conditions set in the reactor on the left.

Experimental Methods

To begin experiments testing the kinetics of low-pH Fe(II) oxidation, a bioreactor first had to be established using the sediment and water collected from the field. The ensuing experiments were started only after sufficient biomass had been produced by the enrichment culture. Once this was the case, different hydrodynamic and geochemical conditions were tested in flow-through mode. Two preliminary experiments determined an optimal hydraulic residence time (θ_h) in the reactor by varying it over a range of values. Two other experiments varying the reactor pH and influent Fe(II) concentration were then performed. The chronology of experiments and their associated methods are discussed in the following sections.

Enrichment Culture 1

Initial phase in flask

After collecting sediment from the site, 25 g of sediment was placed into a sterile bottle which was then filled to a volume of 250 mL with filtered (0.2 micron) Brubaker Run water. This bottle was manually shaken for one minute to try to separate any cells from the sediment. After shaking, the contents of the bottle settled and 100 mL of this inoculum was placed into a 1000 mL Erlenmeyer flask with 900 mL of filtered Brubaker Run water. This mix of sediment, water, a tube to bubble compressed air, and a stir bar spinning at 60 rpm collectively made up the bioreactor in the flask. The inoculum and flask bioreactor are shown in Figure 2-4.

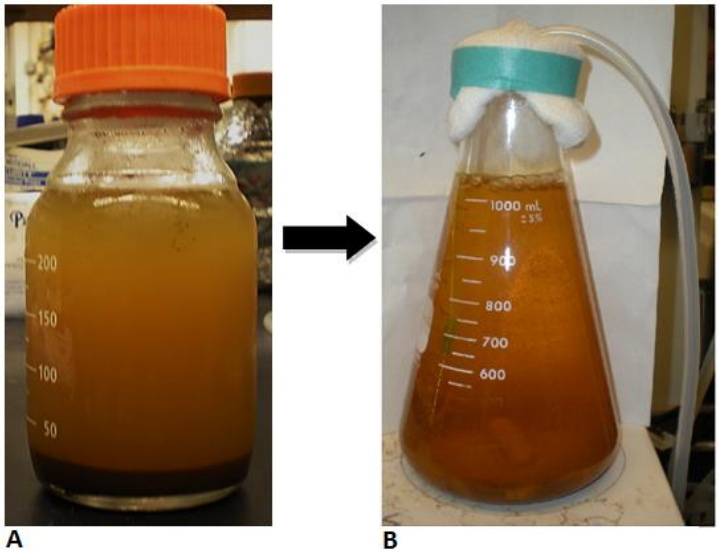

Figure 2-4: (A) The inoculum is shown with the large sediment particles settled at the bottom of the bottle. In (B), the flask has been inoculated and the enrichment culture has begun.

The first phase of this initial enrichment culture in the Erlenmeyer flask was done with less data monitoring than was available in the automated reactors. The concentrations of dissolved Fe(II), total total iron (Fe(T)), and dissolved oxygen, along with the pH, were measured daily. Total Fe(T) is a measurement of the unfiltered concentration of Fe(II) and Fe(III). The pH

was not maintained at a set value, and so it dropped from 3.13 at the start of the culture to 2.26 at the end. Periodic spikes of ferrous sulfate were done to increase the Fe(II) concentration to 150 mg Fe/L. At first, the spikes of Fe(II) did not occur daily because the rate of Fe(II) oxidation was very slow, but by the end the spikes were every day.

Transfer of the culture and continued run time

After 13 days of running in the Erlenmeyer flask, the enrichment culture was transferred to one of the sterile chemostats. Before the contents were transferred, the flask was homogenized by scraping as much of the biofilm off the walls of the flask and increasing the rotation rate of the stir bar. This ensured that as much of the biofilm was transferred as possible. Once transferred, filtered Brubaker Run water was used to bring the volume of the chemostat to 2 L.

From this point forward for this enrichment culture, the automated chemostat's abilities were utilized. The stirring (agitation) rate and pH were kept constant at 50 rpm and 2.9 (by adding sodium hydroxide), respectively. Periodic spikes of a ferrous sulfate solution were done to maintain a sufficient Fe(II) concentration for the microorganisms. One of the pumps on the unit was used to maintain the water level of the reactor at 2 L by pumping out water.

After the transfer to the chemostat, this enrichment culture continued running in the chemostat for another 29 days. A close-up of the biofilm in the chemostat after the enrichment culture is shown in Figure 2-5. By the end of the 29 days, the bioreactor was oxidizing almost all of the 150 mg Fe(II)/L daily, so the reactor was switched into flow-through mode for the first experiment.

Figure 2-5: The orange biofilm was well established in the chemostat after 29 days of running in the enrichment culture mode.

Hydraulic Residence Time Test 1

The first flow-through experiment was performed by varying hydraulic residence times (θ_h) in the chemostat. This was the first of the two preliminary tests to determine an optimal hydraulic residence time for the reactor based on Fe(II) oxidation rates. The residence times were varied in succession from 24 to 12, 6, 3, 1, 0.75, and 0.5 h. After reaching 0.5 h, the θ_h was increased back to 3 h and then to 6 h to see if the reactor could recover from the low θ_h. Each set point was run until the system stabilized with respect to the ratio of the effluent to influent Fe(II) concentrations. The frequency of Fe(II) and Fe(T) measurements depended on the length of θ_h. More measurements were taken at the start of each new θ_h, and after many pore volumes the measurements were less frequent. Other operating parameters for the experiment were pH=2.9, a constant temperature of 20ºC, and a constant agitation of 120 rpm.[4]

During this and all of the other flow-through experiments, the chemostats operated as completely stirred tank reactors (CSTRs) with a biofilm present. Feed water entered the bottom

of the reactor, effluent water was drawn from near the water surface, and sodium hydroxide or sulfuric acid was pumped into the top of the reactor to control pH. The feed water was simply the filtered and stored water that had been previously collected from Brubaker Run. Nitrogen gas was bubbled into the feed container to prevent any oxidation of the Fe(II). The feed container was still either covered in aluminum foil or a cardboard box to prevent possible photooxidation. The tubing periodically had to be replaced because it started to clog with ferric iron precipitates.

Enrichment Culture 2

After the first hydraulic residence time test, the contents of the reactor were discarded and a new enrichment culture was started. The procedure for the inoculum preparation was slightly different this time as compared to the first enrichment culture. Also, for this culture there was no phase of growth in a flask.

To begin the second enrichment culture, 100 g of collected sediment from Brubaker Run was mixed with 900 mL of 0.1% (m/v) sodium pyrophosphate.[1] For 30 minutes, this mixture was stirred at 400 rpm to separate cells from the sediment. A previous study had shaken the mixture for 30 minutes as opposed to using a stirrer.[1] After 30 minutes, this inoculum was allowed to settle and then 1000 mL of the supernatant was poured into a sterile chemostat. The volume of the liquid in the chemostat was increased to 2 L using filtered Brubaker Run water.

After the inoculation of the chemostat, the enrichment culture ran for a total of 30 days. The chemostat controlled the pH at 2.9 and kept the stirring rate at 50 rpm. The reactor was spiked to an Fe(II) concentration of 300 mg/L instead of 150 mg/L , as was the case for the first culture. By the end of the 30 days, the culture required daily doses of Fe(II) because the microorganisms were oxidizing the Fe(II) at a fast rate.

Hydraulic Residence Time Test 2

After the second enrichment culture, a second flow-through test varying the hydraulic residence time of the chemostat was performed. In terms of measurements and set points, the same procedure that was carried out for the first test was mirrored for this one. However, one difference was that after running at θ_h=0.5 h, the θ_h was increased to 1 h and 3 h instead of 3 h and 6 h.

Enrichment Culture 3

A third enrichment culture was needed to run the final two experiments. This enrichment culture varied from the previous two in terms of the inoculum. Instead of using fresh sediment to start this enrichment culture, the homogenized contents of the bioreactor used for the second hydraulic residence time test were used as the inoculum. The process of homogenizing the bioreactor was similar to the homogenization of the flask bioreactor in the first phase of the first enrichment culture. From this inoculum, 1 L was transferred to the second sterile chemostat, leaving 1 L remaining in the first chemostat. Filtered Brubaker Run water was added to each chemostat to bring their volumes to 2 L.

From this point forward, these two simultaneous enrichment cultures were run with the same procedure as the second enrichment culture. One of these eventual bioreactors was to be used in an experiment varying the reactor pH, and the other was to be used in an experiment varying the influent Fe(II) concentration. The only difference between these simultaneous cultures is the length of time each ran before being switched into flow-through mode. The pH experiment's bioreactor ran for 44days, and the influent Fe(II) experiment's bioreactor ran for 83 days. The oxidation rates for the chemostats at the end of the enrichment phase were both in the range of 10-14 mg Fe(II)/L/h, which is also the range of what the second enrichment culture

attained before being switched to flow-through mode. The first enrichment culture reached a similar oxidation rate, but it was slightly lower than this range.

At the end of each of these simultaneous enrichment cultures, a sample of the biofilm and suspension were taken to determine the protein concentrations, and consequently the biomass concentrations, in each phase of the chemostat. These protein measurements would also be taken during the subsequent tests to see how the biomass changed.

Varying Reactor pH Test

After the simultaneous enrichment culture, the reactor intended for the varying pH experiment was switched into flow-through mode. This experiment varied the pH within the chemostat through a series of values with some repeats. The pH started at 2.9 and varied in sequence to 2.6, 2.3, 2.6, 2.9, 3.2, 3.5, 3.8, 4.1, 3.8, and 3.5. The total run time for this test was 84 days, the average influent Fe(II) concentration was 309 mg /L, and the hydraulic residence time was 6 h. The pH in the reactor was set by the addition of either sulfuric acid or sodium hydroxide. Each pH set point was held for at least four days to allow the microbial community to change.[24] The repeat of certain pHs allowed for better rate calculations and also to see how dynamic the system was in terms of the varying pH.

The procedure for measurements during this test was the same as that of the two hydraulic residence time tests. This includes both the frequency and types of measurements. The only difference for this test is that protein measurements of the biofilm and suspension were taken after every pH set point to determine how the biomass concentration changed in terms of its total concentration and distribution between the two phases (biofilm and suspension).

Varying Influent Fe(II) Concentration Test

After the other simultaneous enrichment culture was complete, the flow-through experiment for the varying influent Fe(II) concentration reactor began. The total run time for this test was 60 days, the reactor pH was set at 2.9, and the hydraulic residence time was again 6 h. The influent Fe(II) concentration began at 300 mg /L and varied in sequence to ~80 (non-spiked Brubaker Run water), 300, 600, 1200, 2400, 1200, and 600 mg/L . The influent water in the feed container was spiked with ferrous sulfate to reach each desired concentration. Only the 80 mg/L set point did not need to be spiked because this was the natural concentration of the collected site water. Finally, just as in the varying pH experiment, here each influent Fe(II) concentration set point was run for at least 4 days to allow the microbial community to change.[24]

The same procedure for measurements as that in the varying reactor pH test was used in this test. Protein measurements were again taken to quantify any change in the total biomass concentration and distribution.

Un-inoculated control tests

Three tests were done using sterile and un-inoculated chemostats. These tests were used to verify that the oxidation of Fe(II) that was occurring during all of the previous experiments was in fact biological and not abiotic. First, a test was conducted that varied all of the different HRTs that were used in the two HRT tests. Next, a test was performed that varied the reactor pH stepwise from 2.3 to 2.9 and then to 4.1. These three set points were used in order to cover the entire range of values that were tested in the previous experiment. Finally, a test was conducted that used an influent Fe(II) concentration of 300 and 2400 mg/L. Only two values were used for this last experiment because a third data point was drawn from the hydraulic residence time control test. This data point had the operating conditions of θ_h=6 h, pH=2.90, and an influent

Fe(II) concentration of about 150 mg /L. All of these non-inoculated control tests were run with the same set operating conditions as the tests to which they were meant to be compared. For example, the pH control test had an influent Fe(II) concentration of 300 mg/L.

Analytical Methods

Reactor data logging

During each experiment, data-logging software was used to record all of the set operating conditions, except the air sparger's flow rate. These measurements were taken at every 1 minute interval. This produced very good resolution of the data for the chemostat-controlled variables.

Ferrous and total iron

Many Fe(II) and Fe(T) measurements were taken during each experiment. A colorimetric assay using ferrozine was used to determine the Fe(II) concentrations.[17] The Fe(T) concentrations were determined using the same assay, but only after all of the Fe(III) was reduced to Fe(II) using 0.5 M hydroxylamine in 0.5 M hydrochloric acid. For every measurement, dissolved Fe(II) measurements were performed by filtering the samples (0.2 micron syringe filter). Measurements for Fe(T) were not filtered, and so these were total Fe(T) measurements.

Protein

To determine the concentration of cells in suspension and in the biofilm, a Bio-Rad protein assay kit was used. This is a colorimetric assay that uses Coomassie® Brilliant Blue G-250 dye to determine protein concentrations. In order to perform this assay, any iron in the

samples needed to be dissolved and the cells needed to be lysed. The procedures varied slightly for the biofilm and liquid samples, and each is described in the following sections. Once the protein concentrations were obtained, the derived conversion factor of 0.15×10^{-12} g protein/typical cell was used to convert the mass of protein present to the to the number of cells.[28]

Biofilm protein measurements

An area of at least 1 cm^2 of biofilm was scraped from the wall of the reactor to use for the protein assay. Adobe® Photoshop® software was used to determine the exact area that was removed each time. The collected biofilm was dissolved in 3 mL of 10% (w/v) oxalic acid.[25] Once dissolved, the cells were lysed by placing 1 mL of this mix with 2 mL of 0.2 M sodium hydroxide, and then performing two freeze-thaw cycles on the sample using the -20ºC freezer.[9] The protein colorimetric assay was then performed using the mixture containing the lysed cells.

Liquid protein measurements

For the suspension, 135 mL of reactor liquid was centrifuged (13,000 × g for 10 min) to pelletize the cells.[9] The masses of the Falcon® tubes used for centrifugation were measured before and after to determine the volumes of each pellet. The liquid was then decanted, and 1 mL of 10% (w/v) oxalic acid was used to dissolve the pellet, similar to what was done for the biofilm sample.[25] To lyse the cells, the same sodium hydroxide and freeze-thaw procedure used for the biofilm was used again here.[9] The colorimetric assay was performed using the solution containing the lysed cells.

Statistical Methods

For each operating condition tested during the flow-through experiments, the system reached a steady state with respect to the ratio of the effluent to influent Fe(II) concentrations. In order to deem certain measured points within the steady state and others not, a range of plus and minus 5% of the last measurement was calculated. Any points that fell within the plus or minus 5% range were deemed to be at steady state. This method placed emphasis on the last measured point for each operating condition since all other points for each condition were compared to it. This statistical test showed that the number of points included in the steady state usually differed for each operating condition. This same test was also done for the ratio of the effluent to influent Fe(T) concentrations.

Chapter 3

Results

Experimental variations of hydrodynamic (i.e. varying hydraulic residence time) or geochemical (i.e. varying reactor pH and influent Fe(II) concentrations) variables in the bioreactor allowed steady state conditions to develop with respect to Fe(II) oxidation. A steady state was achieved for all operating conditions. The influent and effluent Fe(II) and Fe(T) concentrations at all of the points for each steady state condition were used to calculate Fe(II) oxidation and Fe(T) precipitation kinetics. This kinetic analysis determined rates of Fe(II) oxidation and Fe(T) precipitation. For the hydraulic residence time tests, only oxidation rates were analyzed.

The number of steady state points was not always the same for each operating condition. In addition to a differing number of points for each operating condition, the number of points considered to be at a steady state with respect to Fe(II) and Fe(T) measurements for each operating conditions were not always the same. Sometimes there were more points considered to be at a steady state for Fe(II), while other times there were more for Fe(T); therefore, the correct points needed to be selected for the oxidation and precipitation rate calculations.

Preliminary Hydraulic Residence Time Tests

These two experiments varied the hydraulic residence time in the reactor over the range of 0.5-24 h. They followed the same procedure and used the same hydraulic residence times, except for one of the repeated hydraulic residence times. Figures 3-1 and 3-2 show the data for the measurements of Fe(II) and Fe(T) for the first and second hydraulic residence time tests, respectively. The x-axis has been normalized to pore volumes for each test.

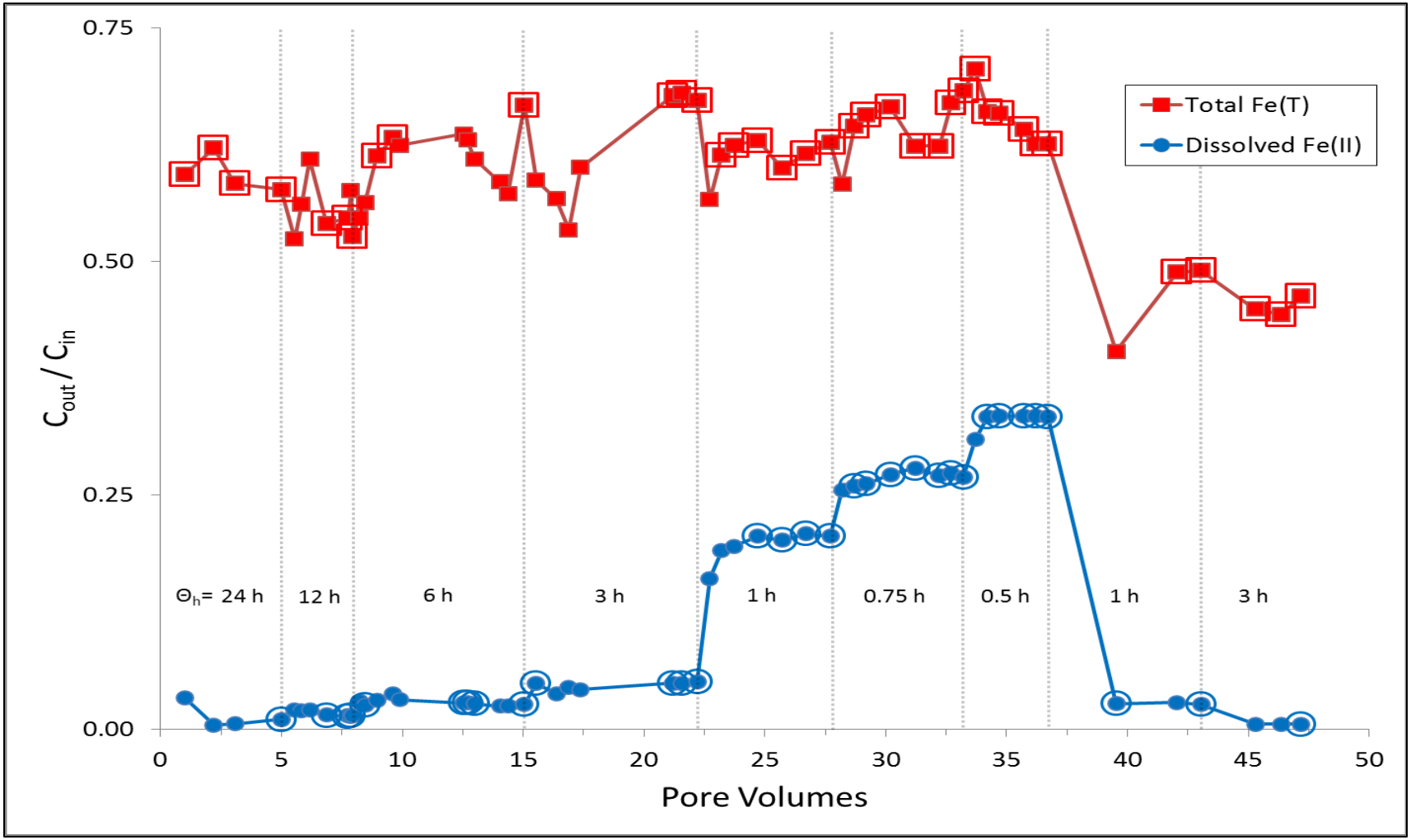

Figure 3-1: The ratios of the effluent to influent concentrations for total Fe(T) and dissolved Fe(II) are shown for the first varying hydraulic residence time test. The θ_h values tested are shown in the regions divided by vertical dashed lines. The large open square and circle markers show the points that were found to be at a steady state for Fe(T) and Fe(II), respectively.

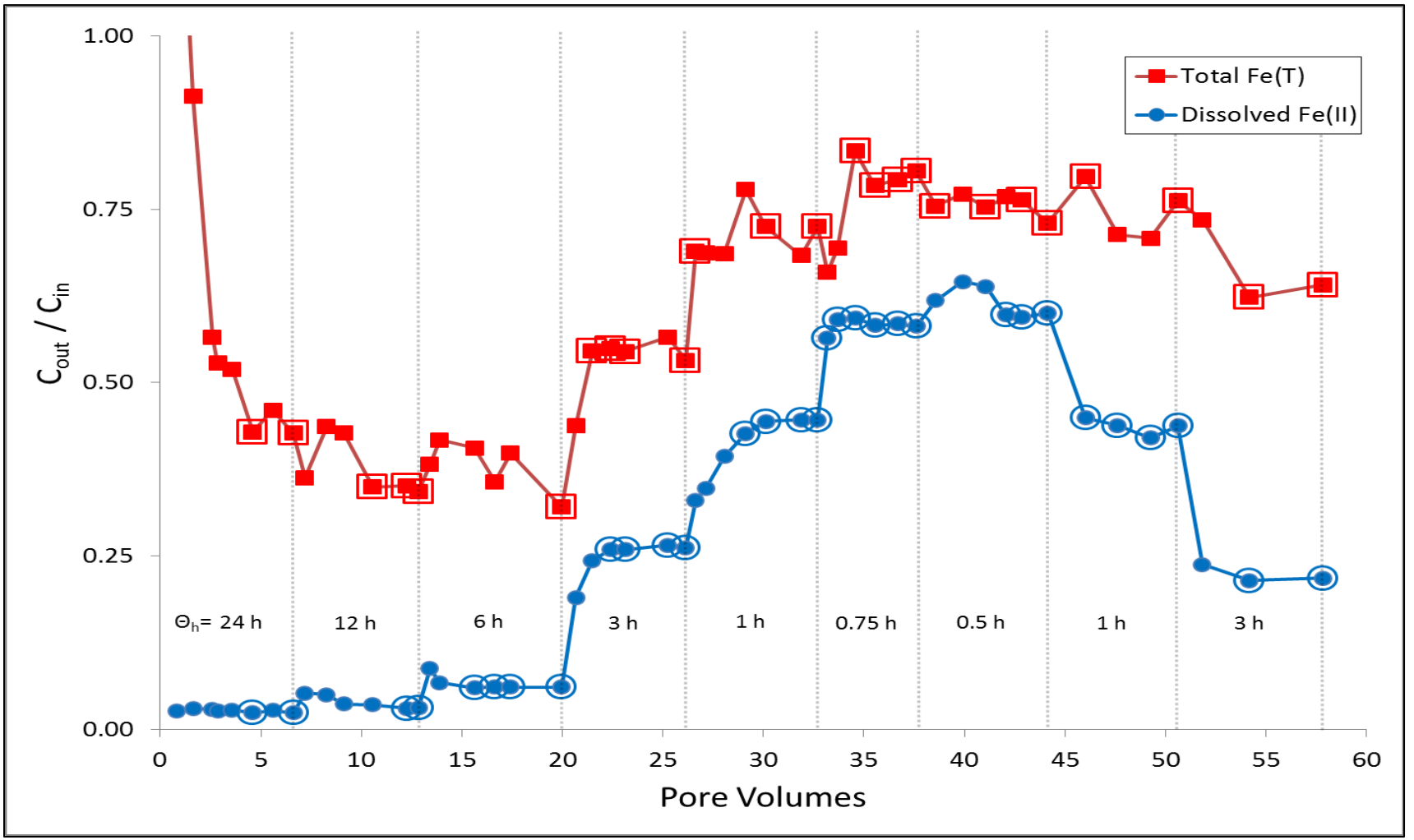

Figure 3-2: The ratios of the effluent to influent concentrations for total Fe(T) and dissolved Fe(II) are shown for the second varied hydraulic residence time test. The large open square and circle markers show the points that were found to be at a steady state for Fe(T) and Fe(II), respectively.

Figures 3-1 and 3-2 provide valuable information about the kinetics in the bioreactor. These plots show that slower flow rates (larger θ_h) cause more Fe(II) to be oxidized, while the reverse is true for faster flow rates (smaller θ_h). From the measured iron data for both of the hydraulic residence time tests, the oxidation efficiencies were calculated at every steady state point (shown as large open circles in Figure 3-2) for each θ_h tested. Equation 3-1 was used to calculate the oxidation efficiency,

$$\text{Oxidation Efficiency (\%)} = \left(\frac{[\text{Fe(II)}_{\text{in}}] - [\text{Fe(II)}_{\text{out}}]}{[\text{Fe(II)}_{\text{in}}]}\right) \times 100 \qquad (\text{Eq. } 3-1)$$

where $[Fe(II)_{in}]$ is the dissolved influent concentration of Fe(II) in (mg/L) and $[Fe(II)_{out}]$ is the dissolved effluent concentration of Fe(II) in (mg/L). These efficiencies are the plotted as a function of the hydraulic residence time in Figure 3-3.

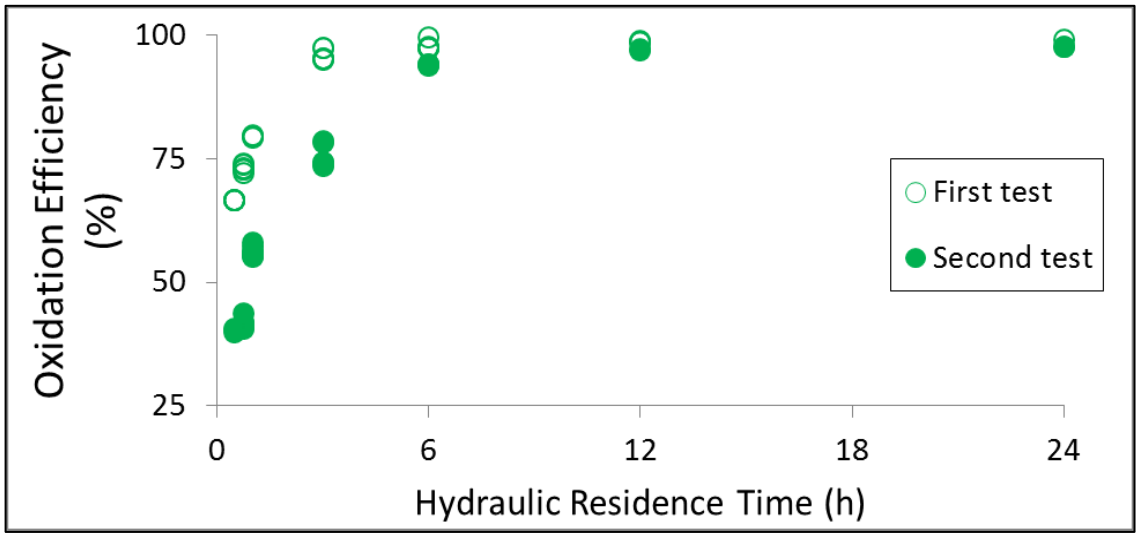

Figure 3-3: The oxidation efficiencies for both tests seem to level off when θ_h is 6 h or greater.

The data for the two experiments yielded similar results, especially at the larger hydraulic residence times. Figure 3-3 shows that the oxidation efficiency levels off and is very close to 100% for both tests when θ_h is 6 h or greater. Therefore, the optimal θ_h was chosen as 6 h, and all subsequent experiments were run with this hydraulic residence time.

Varying Reactor pH Test

After the conclusion of the hydraulic residence time experiments and the third enrichment culture, the two newly produced bioreactors were used to carry out the final experiments. The first one was the varying reactor pH test. Figure 3-4 shows this experiment's measured iron data, similar to Figures 3-1 and 3-2.

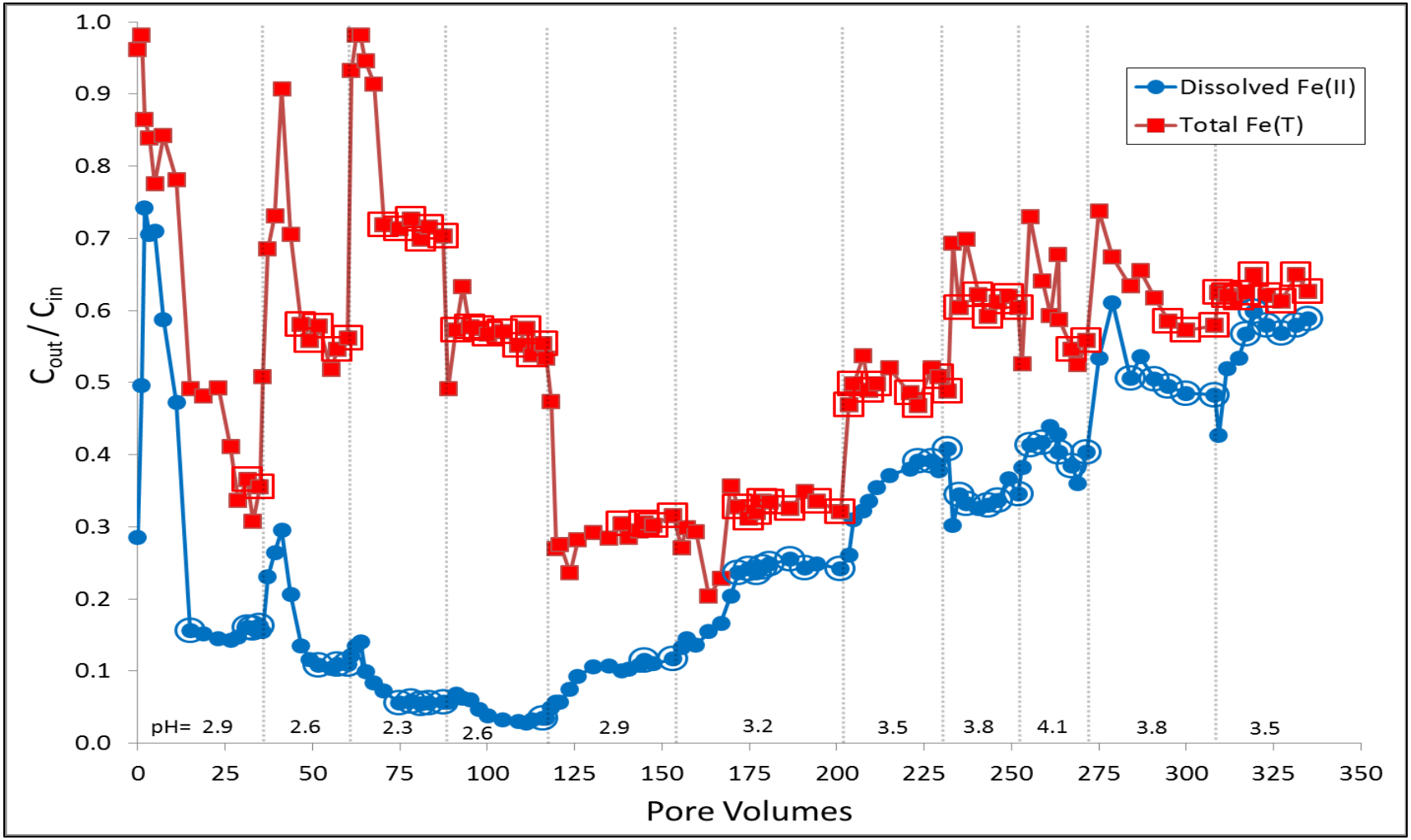

Figure 3-4: The ratios of the effluent to influent concentrations for total Fe(T) and dissolved Fe(II) are shown for the varying reactor pH experiment. The large open square and circle markers show the points that were found to be at a steady state for Fe(T) and Fe(II), respectively.

At every steady state point (shown as open circles squares in Figure 3-4) for each pH set point, oxidation and removal rates were calculated using Equations 3-2 and 3-3,

$$R_{oxidation} = \left(\frac{[Fe(II)_{in}] - [Fe(II)_{out}]}{\theta_h}\right) \quad (Eq. 3-2)$$

$$R_{removal} = \left(\frac{[Fe(T)_{in}] - [Fe(T)_{out}]}{\theta_h}\right) \quad (Eq. 3-3)$$

where $R_{oxidation}$ is the oxidation rate in (mg Fe(II)/L/h), $R_{removal}$ is the removal rate in (mg Fe(T)/L/h), $[Fe(T)_{in}]$ is the total influent concentration of Fe(T) in (mg Fe(T)/L), and $[Fe(T)_{out}]$ is the total effluent concentration of Fe(T) in (mg Fe(T)/L) . Figures 3-5 and 3-6 show the oxidation and removal rates plotted as a function of the rector pH, respectively. These two figures show data for both the varying reactor pH and influent Fe(II) concentration tests because they have the same operating conditions with respect to θ_h, reactor pH, and influent Fe(II) concentration.

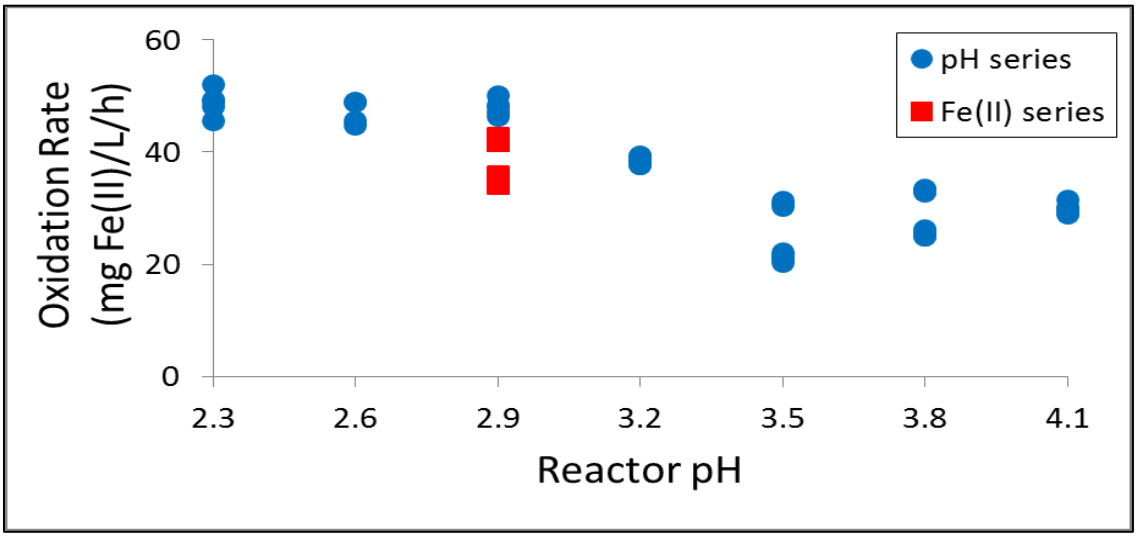

Figure 3-5: The oxidation rate increases as the reactor pH decreases.

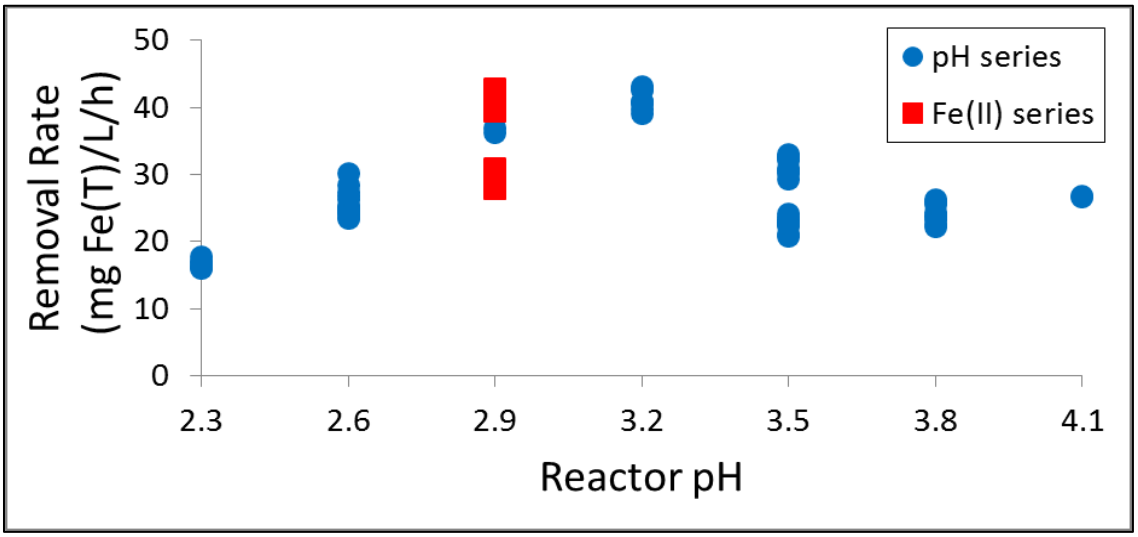

Figure 3-6: The removal rate appears to peak at a reactor pH of 2.9 and 3.2.

The previous two figures plotting the rates of oxidation and removal show important results. First, Figure 3-5 shows an increasing oxidation rate as pH decreases. For the removal rates, the trend shown in Figure 3-6 is surprising. The removal rate was expected to continue increasing with pH, not reach a maximum around 2.9-3.2 and then begin decreasing. Both of these results are important for the kinetic analyses in Chapter 4.

The other measurements taken for this experiment were biomass concentrations of the biofilm and suspension. These measurements were taken at the end of each reactor pH set point, when the system was considered to be at a steady state. After taking into account a conversion factor for the average mass of protein per cell (as previously stated in Chapter 2), these measurements yielded values for the total biomass concentrations in the reactor and the distribution of the biomass between the two phases (biofilm and suspension). These results are shown in Figures 3-6 and 3-7. These plots show that the biomass concentration is relatively stable, with almost all of it present in the biofilm.

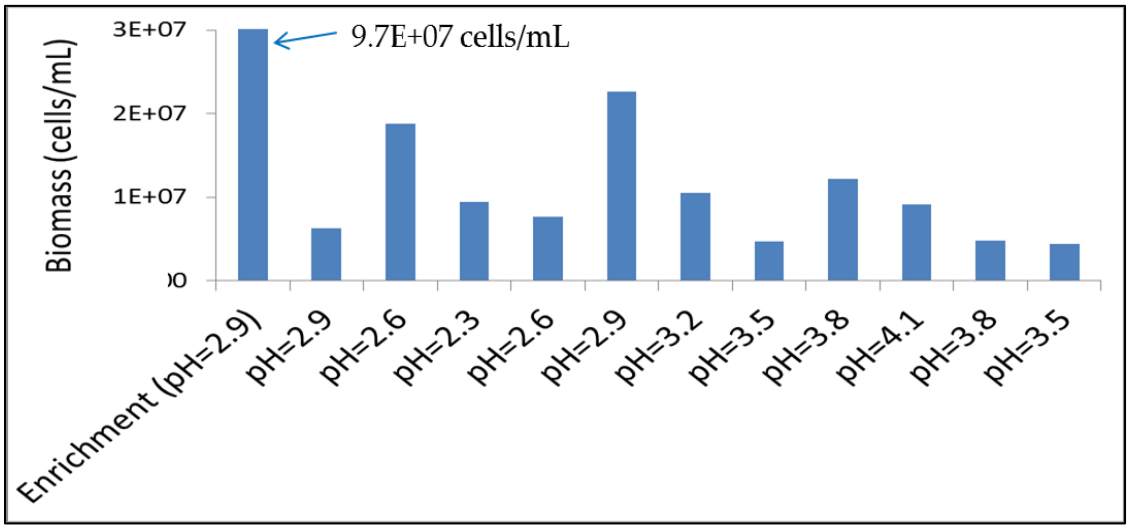

Figure 3-7: The total biomass concentration in the reactor is shown as a function of the reactor pH. The concentrations are relatively steady over the range of pHs.

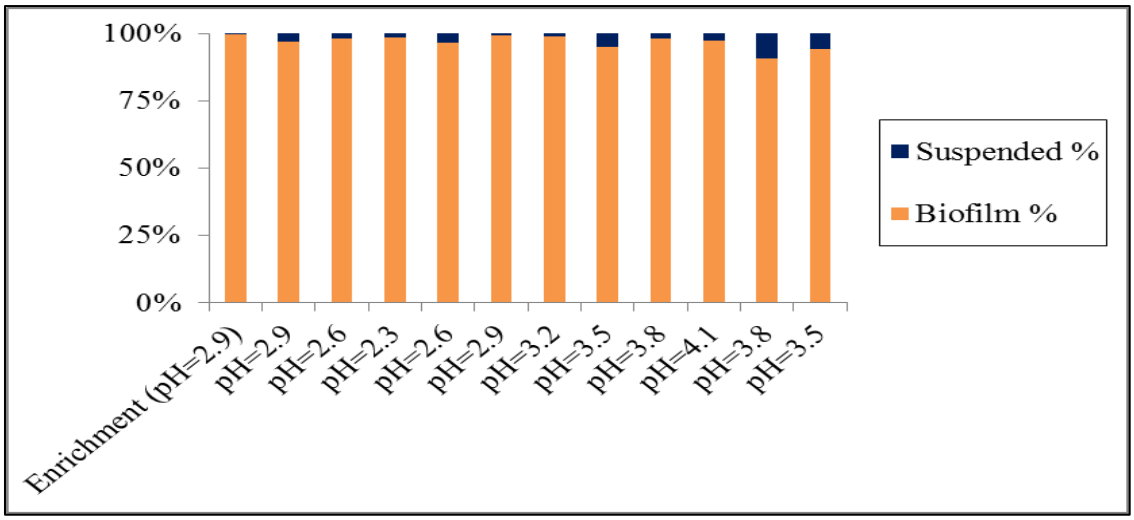

Figure 3-8: At every pH set point, the biomass appears to be present almost entirely in the biofilm, with very little in suspension.

Varying Influent Fe(II) Concentration Test

The final experiment varying the influent Fe(II) concentration used the second bioreactor created during the third enrichment culture. Measured iron concentrations were collected for this experiment and are shown in Figure 3-9.

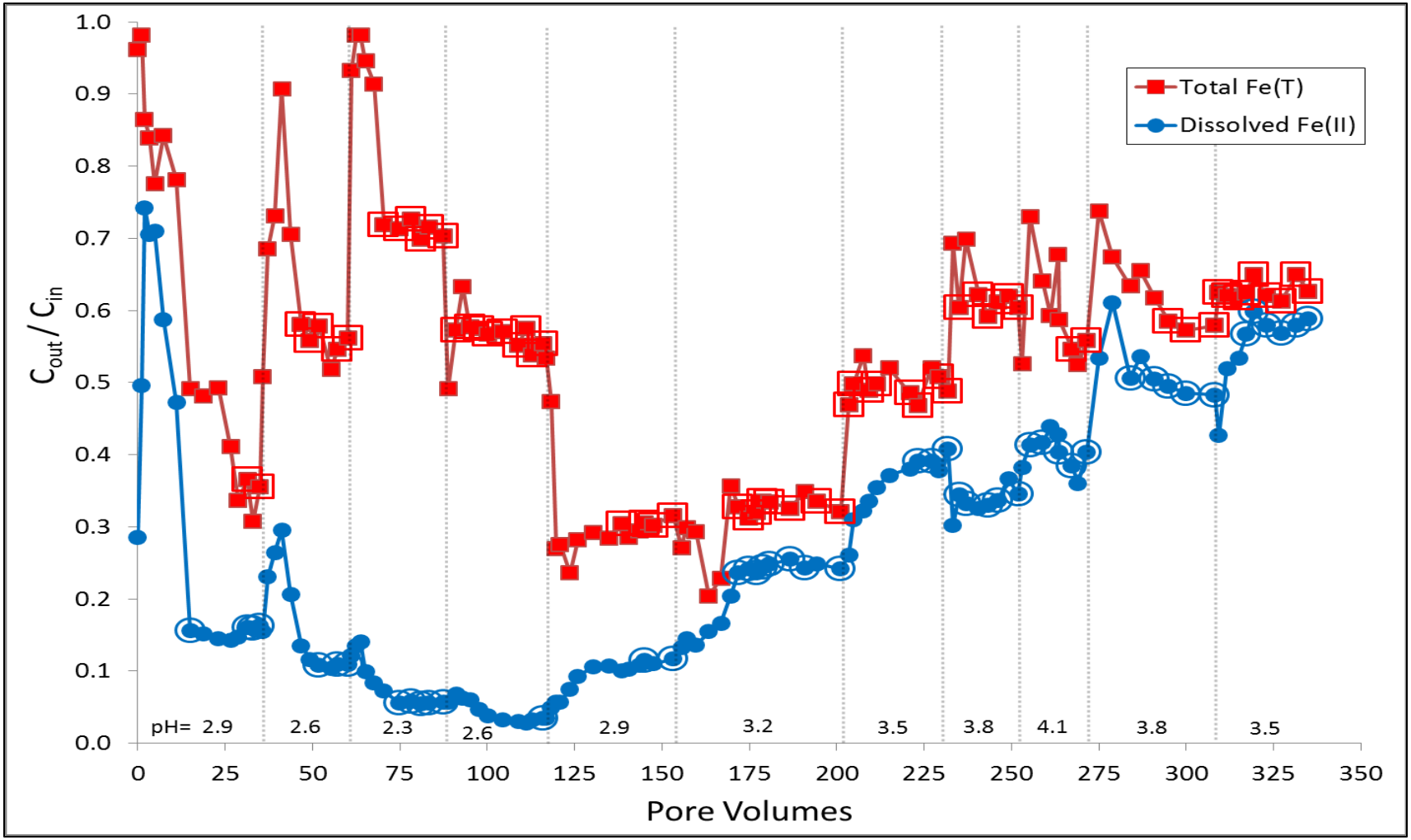

Figure 3-9: The ratios of the effluent to influent concentrations for total Fe(T) and dissolved Fe(II) are shown for the varying influent Fe(II) concentration test. The large open square and circle markers show the points that were found to be at a steady state for Fe(T) and Fe(II), respectively

From the data, Equations 3-2 and 3-3 were again used to calculate oxidation and removal rates. Similar to the last section, Figures 3-10 and 3-11 show plots for the oxidation and removal rates as a function of the effluent Fe(II) concentration, respectively. Although the influent Fe(II) concentration was varied, the effluent concentration of Fe(II) represented the available substrate for the microorganisms (the effluent concentration equals the concentrations in the reactor for a CSTR). Some data from the varying hydraulic residence time and reactor pH tests are included in Figures 3-10 and 3-11 because the operating conditions with respect to θ_h, reactor pH, and influent Fe(II) concentration were the same.

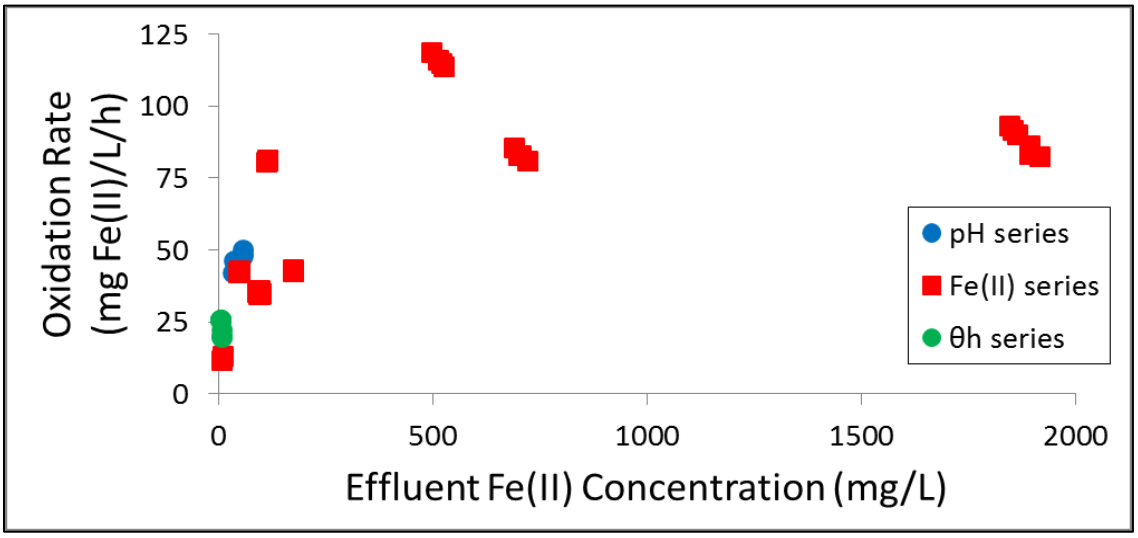

Figure 3-10: The oxidation rate increased with an increasing effluent Fe(II) concentration and appeared to reach a maximum.

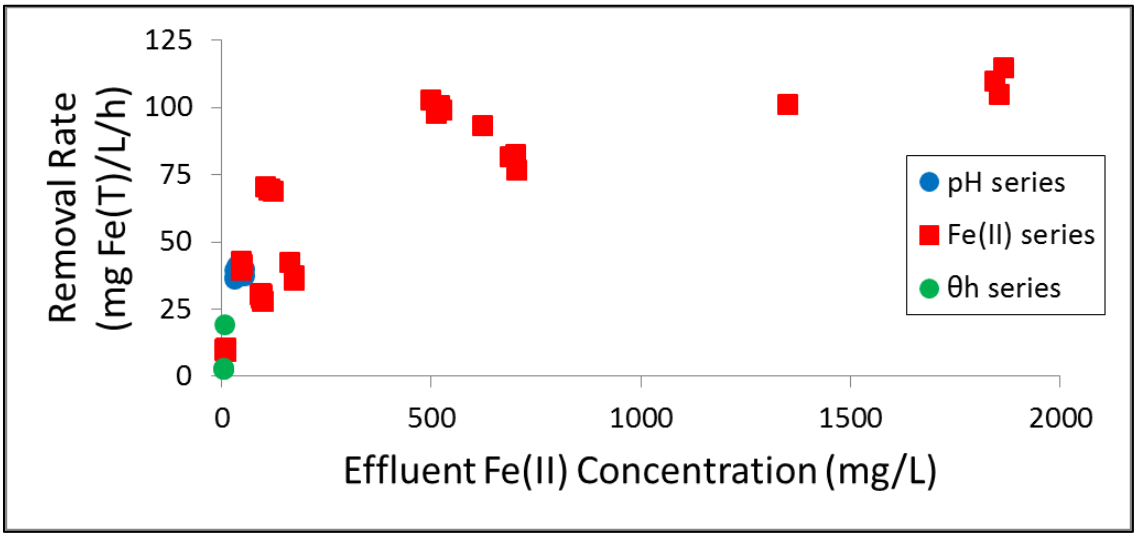

Figure 3-11: The removal rates also increased with increasing effluent Fe(II) concentrations, and again there seemed to be a maximum rate.

The data for this experiment shows important trends. As the effluent Fe(II) concentration is increased, the oxidation rate appeared to reach a maximum and then start decreasing. This could possibly be due to substrate inhibition, and this will be discussed in Chapter 4. The removal rate increased as a function of the effluent Fe(II) concentration and there appeared to be a saturation-like effect on the rate from the Fe(II) in the reactor.

Finally, for this experiment the biomass concentration was measured at the end of each influent Fe(II) concentration set point. Both the total biomass concentration in the reactor and the distribution of the biomass are plotted for each influent Fe(II) concentration in Figures 3-12 and 3-13, respectively. Two biomass measurements were taken during the enrichment phase before this experiment started, and these are marked as "Enrichment" with their corresponding sample dates in parentheses. Similar to the other biomass measurements, the ones for this experiment show that the biomass concentration was generally stable, with most of it being present in the biofilm. The least amount of biomass was present at the highest concentrations of influent Fe(II), which could be attributed to cell inhibition due to the precipitation of iron solids within the reactor.

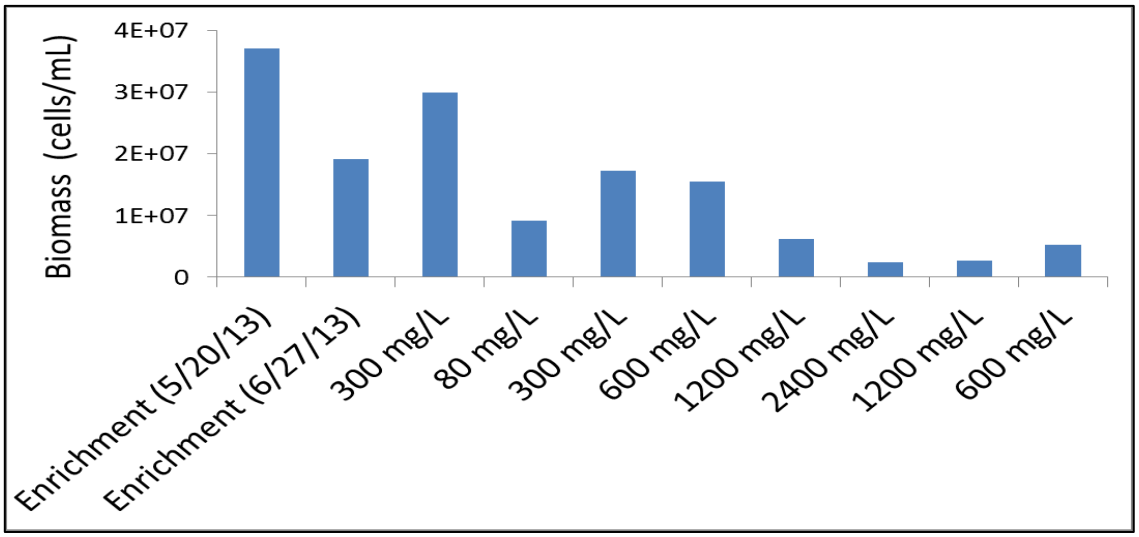

Figure 3-12: The biomass concentration appears to be relatively stable. The decrease in concentration toward the end of the experiment could be due to the cumulative amount of samples taken from the reactor.

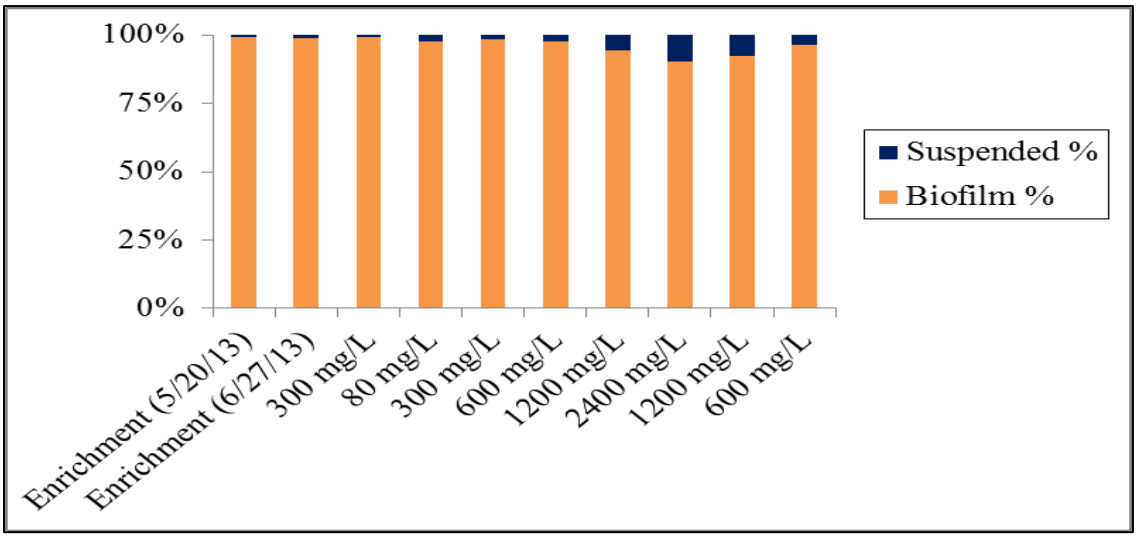

Figure 3-13: The majority of the biomass is in the biofilm, with only a small amount in suspension.

Un-inoculated Control Tests

The un-inoculated control tests verified that the observed Fe(II) oxidation was biological and not abiotic. All of the controls had less than 5% oxidation of the influent Fe(II) to the reactor. The control for the varying reactor pH test had the most abiotic oxidation out of all of the controls when the pH was 4.1; however, this was still less than 5%.

Chapter 4

Discussion

Optimal Fe(II) Oxidation Conditions

The experiments varying the reactor pH and influent Fe(II) concentration show important operating conditions for the bioreactor. In order to achieve optimal Fe(II) oxidation, Figures 3-5 and 3-10 showed that the bioreactor should be run with a low-pH and high influent Fe(II) concentration, respectively. The oxidation rate appears to begin to level off when pH is decreased to 2.6 and 2.3. As was stated in Chapter 1, two previous studies found no effect from pH on the Fe(II) oxidation rates over the ranges of 1.3-2.2[13] and 1.5-2.5;[18] therefore, the possible leveling off of the rate at the lowest pH set points would agree with those studies. The oxidation rate appeared to reach a maximum when the effluent Fe(II) concentration was about 900 mg/L, and the rate decreased as the Fe(II) concentration was increased this concentration. However, even though the rate decreased above an effluent Fe(II) concentration of 900 mg/L, these rates were generally still greater than those achieved at the lower concentrations. These operating conditions are important to consider when implementing this type of bioreactor at different AMD sites that each have their own unique geochemistry.

Rate Equation for Fe(II) Oxidation

Rate law derivation

In order to predict Fe(II) oxidation rates in the bioreactor, a rate law must be derived. A general rate law can be written for biological Fe(II) oxidation, and it is shown as Equation 4-1,

$$\mathrm{R_{oxidation}} = \mathrm{k_{bio}} \mathrm{C_{bacteria}^{\alpha}} [O_2]^{\beta} [\mathrm{H^+}]^{\gamma} [\mathrm{Fe(II)}]^{\delta} \qquad (\mathrm{Eq.}\, 4-1)$$

where, k_{bio} is the biological rate constant with units of (mg Fe(II)/L/h)·(mL/cells)$^{-\alpha}$·(L/mg O_2)$^{-\beta}$·(L/mol H^+)$^{-\gamma}$·(L/mg Fe(II))$^{-\delta}$, and α, β, γ, and δ are all theoretical reaction orders for the various terms. The general rate law can be simplified after examining each term. To do this, the oxidation rates can be plotted as a function of each variable to determine if there is any correlation. If there is in fact a relationship present, it can be transformed into a mathematical function and substituted into the general rate law equation. This procedure is performed in the following paragraphs.

The concentration of bacteria in the bioreactor does not appear to be correlated to the measured oxidation rates for either experiment. This is evident by the plot in Figure 4-1(A). The rate law model, derived in this section and shown in full later, was also used to calculate oxidation rates that were plotted as a function of the concentration of bacteria. This is shown in Figure 4-1(B). Since both the measured and modeled rates do not seem to be correlated well to the concentration of bacteria, the $C_{bacteria}$ term in the equation will be removed.

As was reported in the results section, the concentration of bacteria in the reactor was relatively constant, but it is interesting to note the magnitude of the rates for the highest and lowest concentrations of bacteria in Figure 4-1(A). The lowest concentrations yield some of the highest rates, while the highest concentration yields a much lower rate. A possible explanation for this is that the different operating conditions selected for different bacteria which were capable of different ranges of oxidation rates. The bacteria present at the lowest concentration might have had the ability to quickly oxidize Fe(II), despite their overall lower numbers.

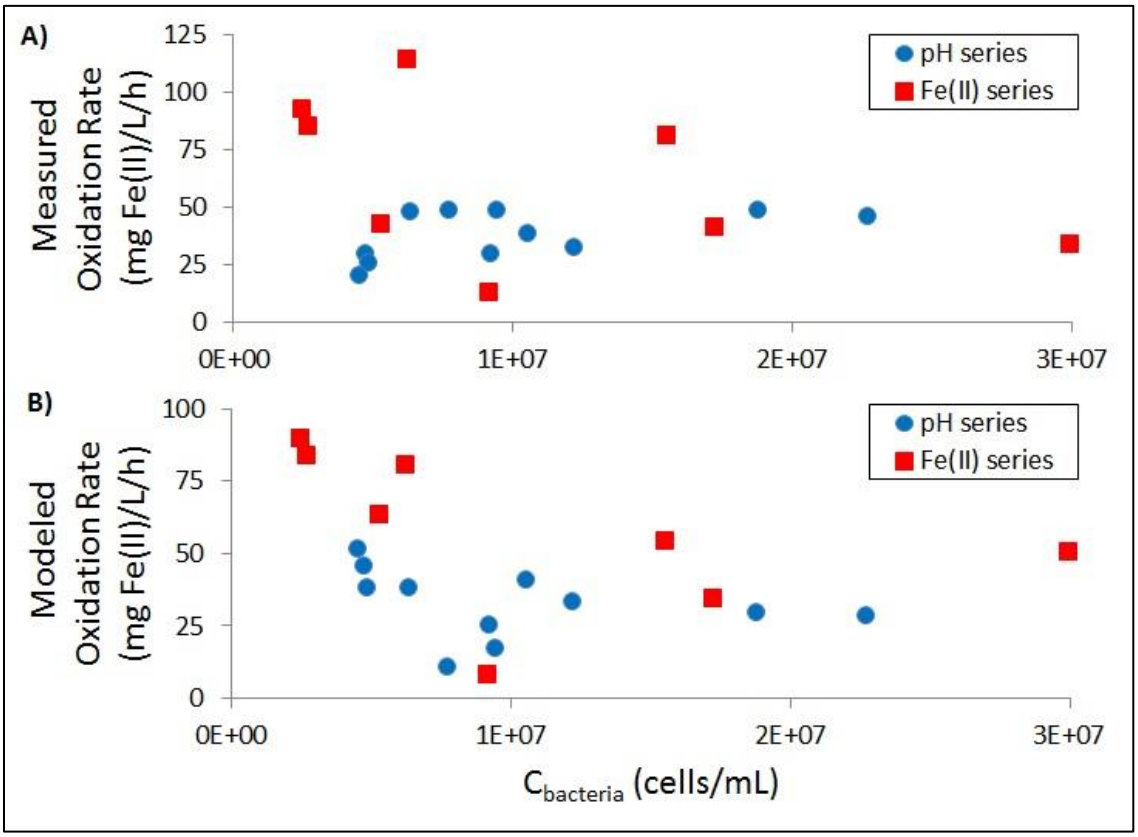

Figure 4-1: The measured (A) and modeled (B) oxidation rates do not correlate well with the bacteria concentration.

Similar to the concentration of bacteria, the dissolved oxygen concentration in the reactor does not correlate well with the oxidation rates. Again, the measured and modeled rates are plotted, and they are shown in Figure 4-2 (A) and (B), respectively. The two vertical dashed lines at $[O_2]$=0.64 and 2 mg/L show two thresholds that were reported in the literature.[6,20] Above these concentrations, the dissolved oxygen concentration is not limiting. All but one measured value had a dissolved oxygen concentration greater than 2 mg/L, and this point was still above the threshold of 0.64 mg/L. Since the measured dissolved oxygen concentrations were always above the threshold limits and since there appeared to be no correlation for the measured or modeled data, the rate equation will no longer include a term for dissolved oxygen.

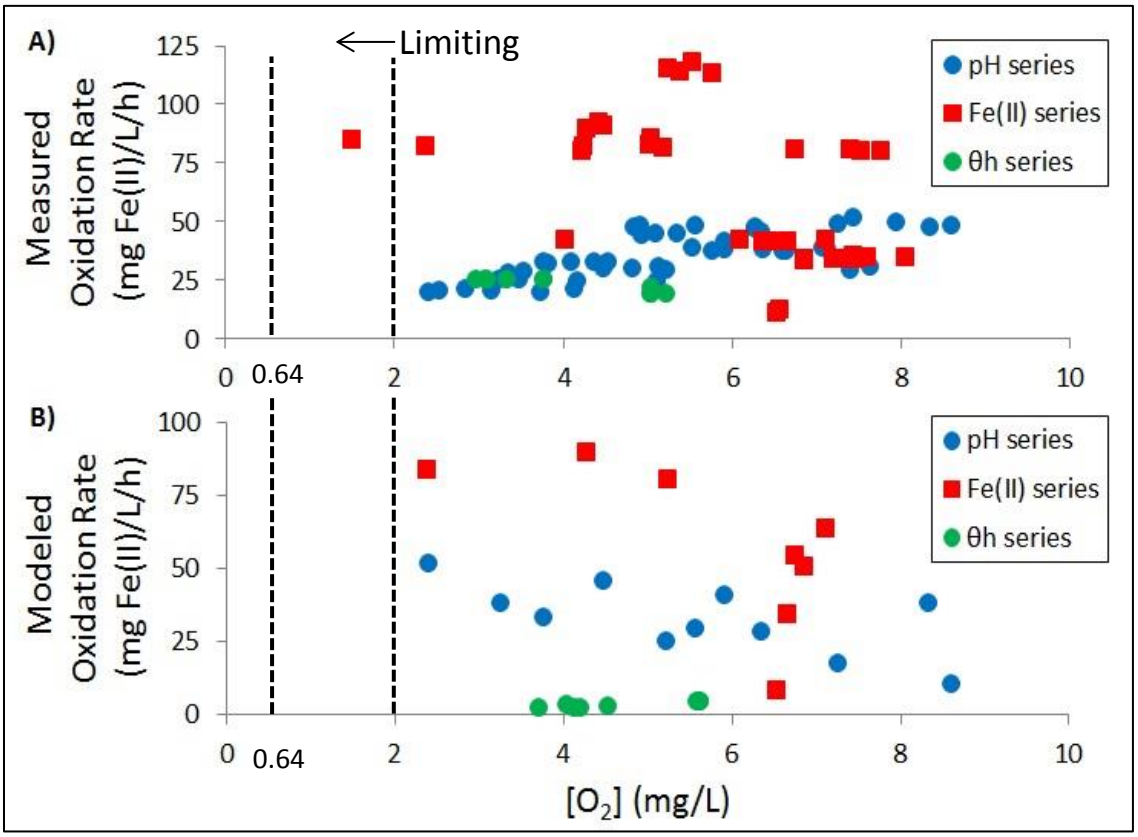

Figure 4-2: The measured (A) and modeled (B) oxidation rates do not correlate well with the dissolved oxygen concentration.

The rate law equation can be simplified by removing the terms for the concentration of bacteria and dissolved oxygen. This simplified equation, Equation 4-2, shows only a dependence on the concentrations of hydrogen ions and Fe(II),

$$R_{oxidation} = k_{bio}[H^+]^{\gamma}[Fe(II)]^{\delta} \qquad (Eq.\,4-2)$$

where, k_{bio} now has the units of (mg Fe(II)/L/h)·(L/mol H+)$^{-\gamma}$·(L/mg Fe(II))$^{-\delta}$).

The term for the hydrogen ion concentration will now be examined. Figure 3-5 previously showed the oxidation rate as a function of reactor pH, and there seemed to be a saturation-like effect on the rate at the lower pH set points. This saturation effect appears again when the oxidation rate is plotted as a function of $[H^+]$. Figure 4-3 shows this plot, along with a Monod curve fitting the data. The Monod curve takes the form of Equation 4-3,

$$R_{oxidation} = \frac{V_{max}[H^+]}{K_{H+} + [H^+]} \qquad (Eq. 4-3)$$

where V_{max} is the maximum oxidation rate in (mg Fe(II)/L/h) and K_{H+} is the half-saturation coefficient in (mol H^+/L). From the Monod curve fitting, the values for V_{max} and K_{H+} are 43.9 mg/L/h and 8.95 x10^{-5} mol/L (pH=4.05), respectively. An important note for this plot is that the fitting is only valid over the range of hydrogen ion concentrations shown. If [H^+] continues to increase (pH decrease), at some point the rate should go down simply because the bacteria would be unable function in that acidic of an environment.

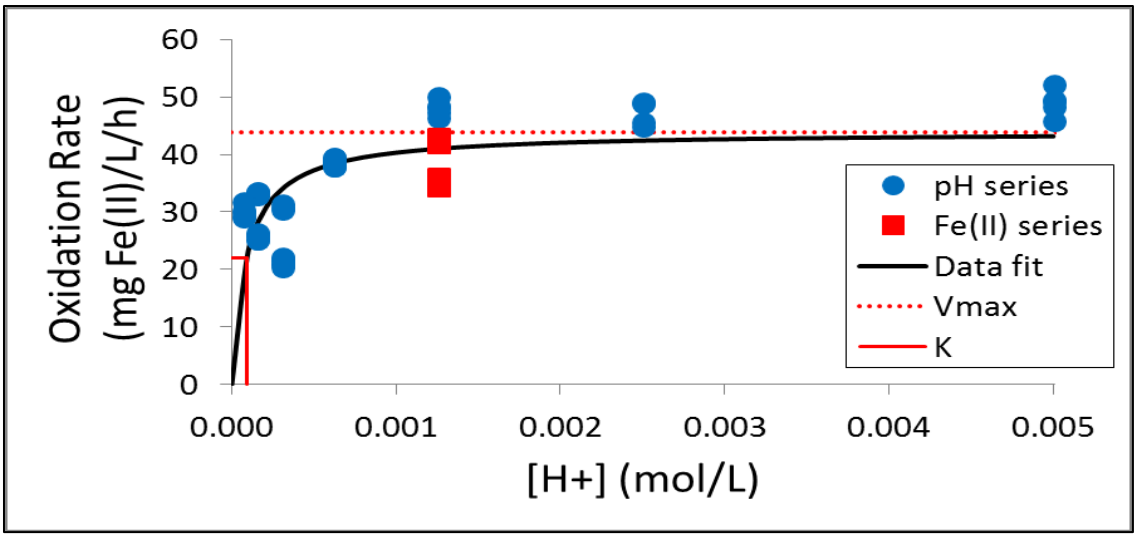

Figure 4-3: The saturation effect of [H^+] on the oxidation rate allows a Monod curve to fit the data. From the fit, V_{max} and K_{H+} were determined.

The rate law equation can now be further simplified by substituting the Monod term for the hydrogen ion concentration term. The V_{max} term is removed from the Monod term and lumped into k_{bio}, which produces a new rate constant, k^*_{bio}. This new form of the rate law is shown in Equation 4-4,

$$R_{oxidation} = k^*_{bio}\left(\frac{[H^+]}{K_{H^+} + [H^+]}\right)[Fe(II)]^{\delta} \qquad (Eq. 4-4)$$

where k^*_{bio} has the units of ((mg Fe(II)/L/h)·(L/mg Fe(II))$^{-\delta}$)

A substitution for the $[Fe(II)]^{\delta}$ term in the rate law equation is the last step in the simplification process. The plot of the oxidation rate as a function of the influent Fe(II) concentration was previously shown in Figure 3-10, and this plot showed another saturation-like effect on the rate. Again, data for the varying hydraulic residence time test at θ_h=6 h were included with the influent Fe(II) concentration data because they all had pH=2.9. A Monod curve can be fit to this data. Figure 4-4 shows this plot with the curves for the fit, V_{max}, and $K_{Fe(II)}$. Similar to K_{H+}, $K_{Fe(II)}$ is the half-saturation coefficient, but it has the subscript Fe(II) to denote it is for the fit of this particular data. The V_{max} and corresponding $K_{Fe(II)}$ values are 97.1 mg/L/h and 69.6 mg/L, respectively.

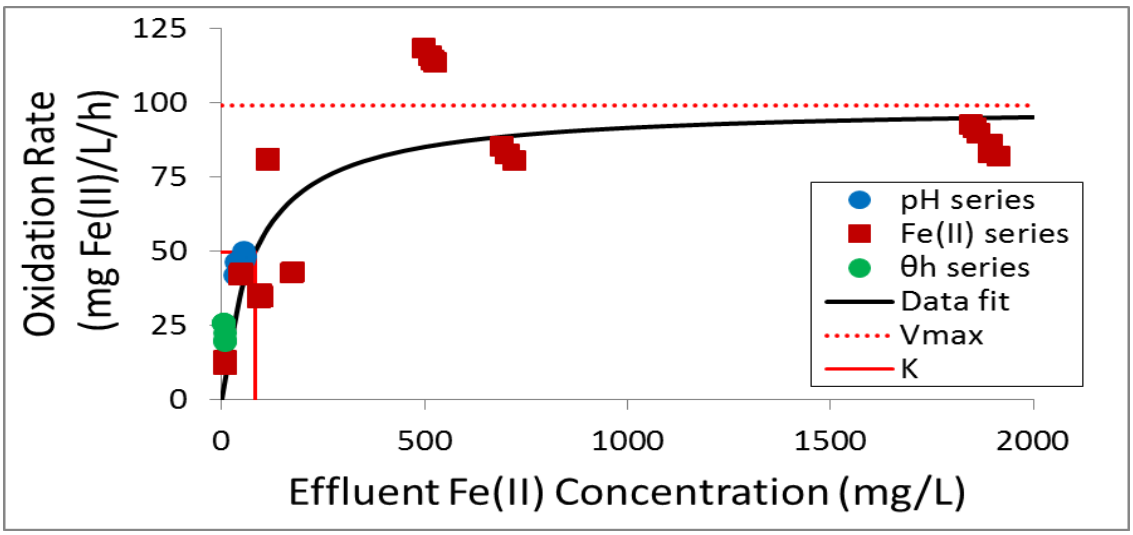

Figure 4-4: A Monod curve fits the saturation-like effect of the effluent Fe(II) concentration on the oxidation rate.

The final rate law equation, Equation 4-5, is found after substituting the Monod term for the $[Fe(II)]^{\delta}$ term,

$$R_{oxidation} = k^*_{bio}\left(\frac{[H^+]}{K_{H^+} + [H^+]}\right)\left(\frac{[Fe(II)]}{K_{Fe(II)} + [Fe(II)]}\right) \qquad (Eq.\ 4-5)$$

where k^*_{bio} has the units of (mg Fe(II)/L/h). The V_{max} from the influent Fe(II) concentration term is lumped into k^*_{bio}, just as was done for the $[H^+]$ term. In order to determine k^*_{bio} for the rate law

equation, the rates are plotted in Figure 4-5 as function of the two Monod terms, and the slope of the linear fit is k^*_{bio}. The resulting k^*_{bio} is 102 mg/L/h.

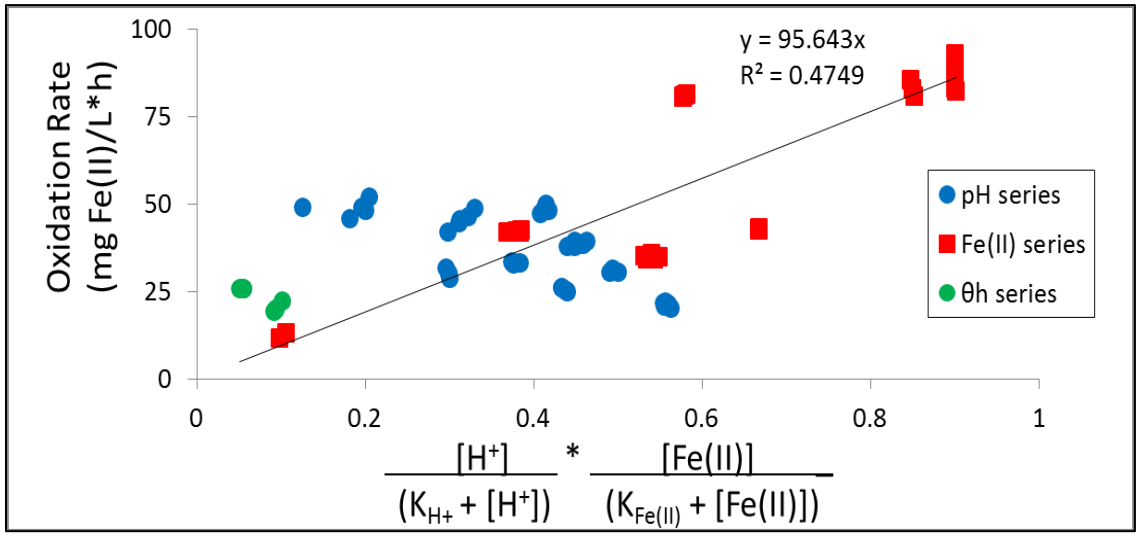

Figure 4-5: The rate constant is found by plotting the two components of the final rate law equation against each other for all of the data. The linear fit was forced through the origin.

Model predicting oxidation rates

The finalized rate law equation in the last section can be used as a model to try to predict the oxidation rates in the bioreactor. The same steady state points chosen for rate calculations in both experiments are used to compare with the model. A plot of the percent error between the model and actual data shows the regions where the model over-predicts (positive percent error) and under-predicts (negative percent error) the rates. Figure 4-6 shows the model, actual data, and percent errors for the varying reactor pH experiment. For the varying influent Fe(II) concentration experiment, the plot of the model, actual data, and associated percent errors are shown in Figure 4-7. The plots appear to show that the model was more accurate for predicting the rates for the varying influent Fe(II) concentration experiment, but there was still a large amount of error. Therefore, more data and possibly more components need to be included in the

rate law equation in order to refine the model. The goal is ultimately to have a model that can have the [H^+] and Fe(II) concentrations at any AMD site as inputs and accurately predict the oxidation rates that can be expected using this type of bioreactor.

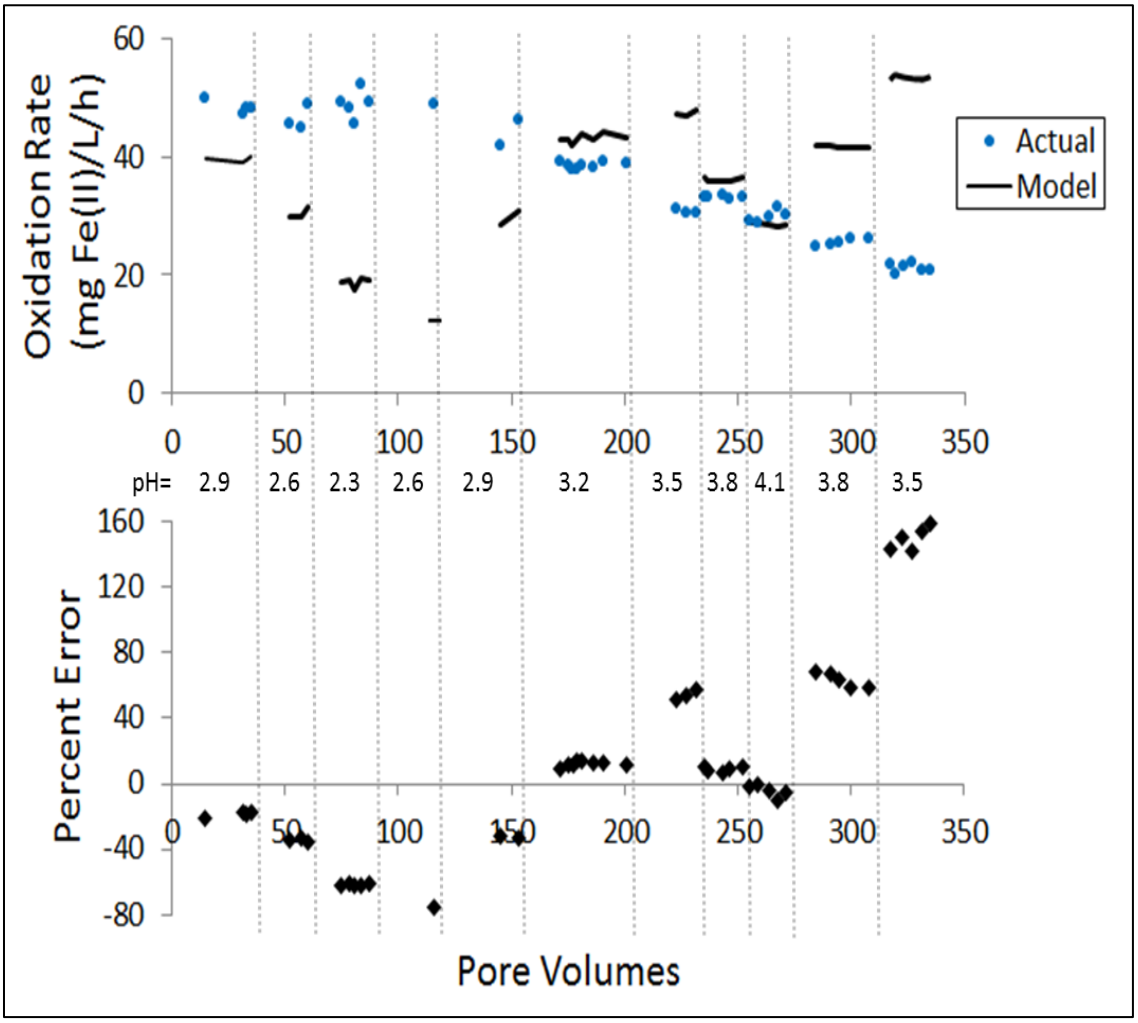

Figure 4-6: The rates predicted by the model for the varying reactor pH experiment show a large amount of error, especially for the larger pH set points.

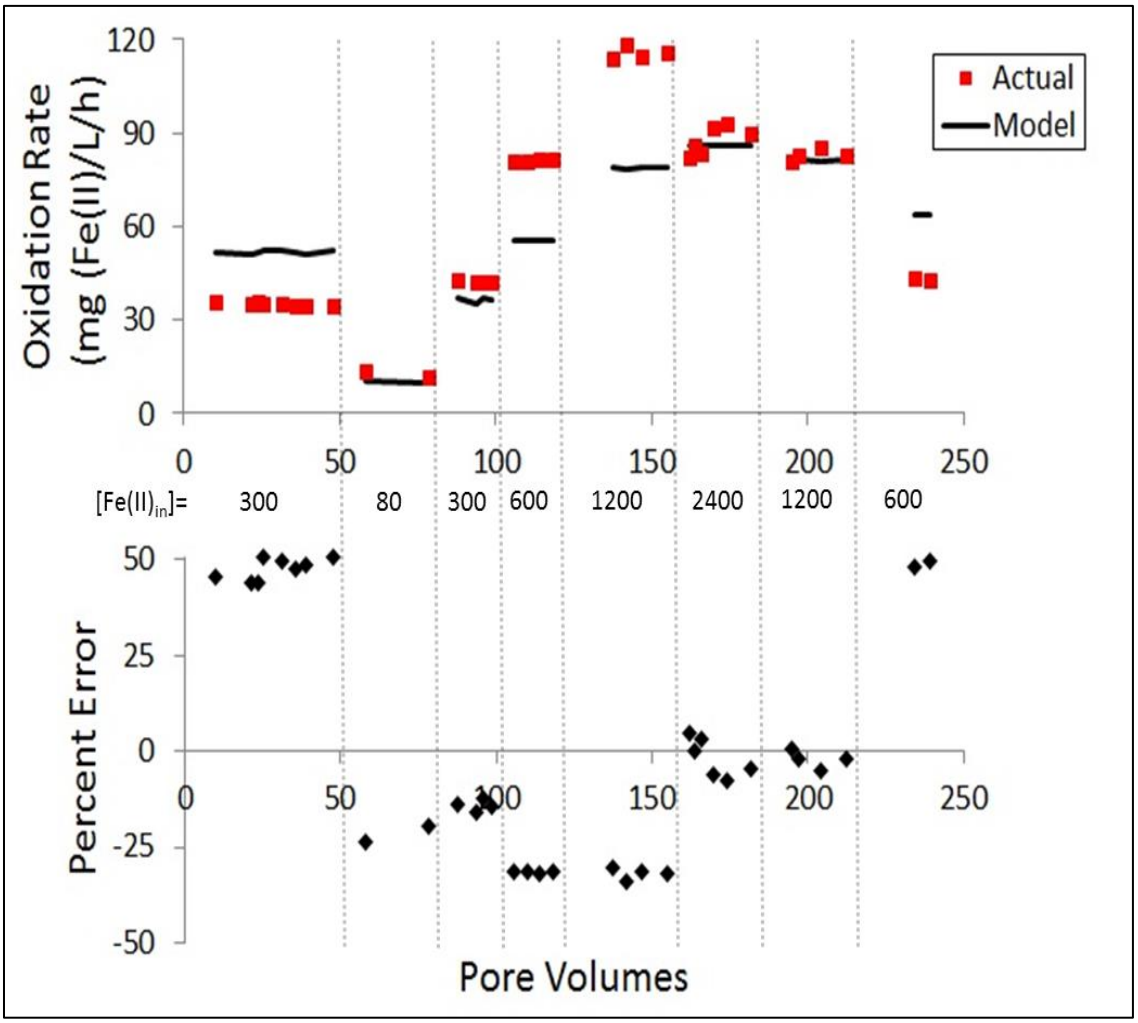

Figure 4-7: The rates predicted by the model for the varying influent Fe(II) concentration experiment are slightly more accurate than those for the varying reactor pH experiment.

Predominant Reactions Occurring in the Bioreactor

The two main reactions that are occurring in the bioreactor are the oxidation of Fe(II) and the precipitation of Fe(III), which were previously shown as Reactions 2 and 4.

$$Fe^{2+} + \frac{1}{4}O_2 + H^+ \leftrightarrow Fe^{3+} + \frac{1}{2}H_2O \qquad \text{(Reaction 2)}$$

$$Fe^{3+} + 3H_2O \leftrightarrow Fe(OH)_3(s) + 3H^+ \qquad \text{(Reaction 4)}$$

These two reactions show that when Fe(II) is oxidized, acidity (H^+) is consumed, and when Fe(III) precipitates, acidity is produced. Therefore, at the steady state condition for each operating condition, the recorded acid and base addition needed to maintain a constant pH in the reactor can be used to help determine which reaction is occurring.

The data for the varying reactor pH and influent Fe(II) concentration experiments are used for this analysis. In order to determine whether only oxidation, or both oxidation and precipitation were occurring, the oxidation rate can be plotted versus the rate at which either acid or base was added. The rate of acid and base addition was used instead of the total volume of acid and base because there were different run times for each steady state point; therefore, this was resolved by normalizing the volumes to rates by using their run times. Figures 4-8 and 4-9 show these plots for the varying reactor pH and influent Fe(II) concentration experiment, respectively.

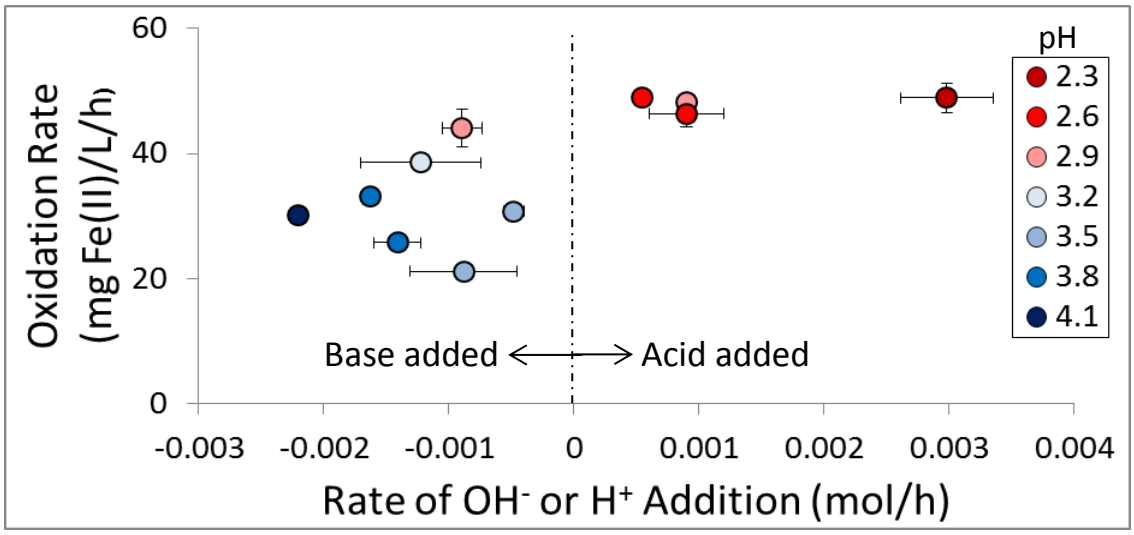

Figure 4-8: The oxidation rate is the highest for the reactor pH set points that required acid addition. Acid addition is evidence of the production of soluble Fe(III) from Fe(II) (Reaction 2), while base addition is evidence for Fe(III) precipitation (Reaction 4). To the right of zero on the x-axis is the acid addition rate, and to the left is the base addition rate.

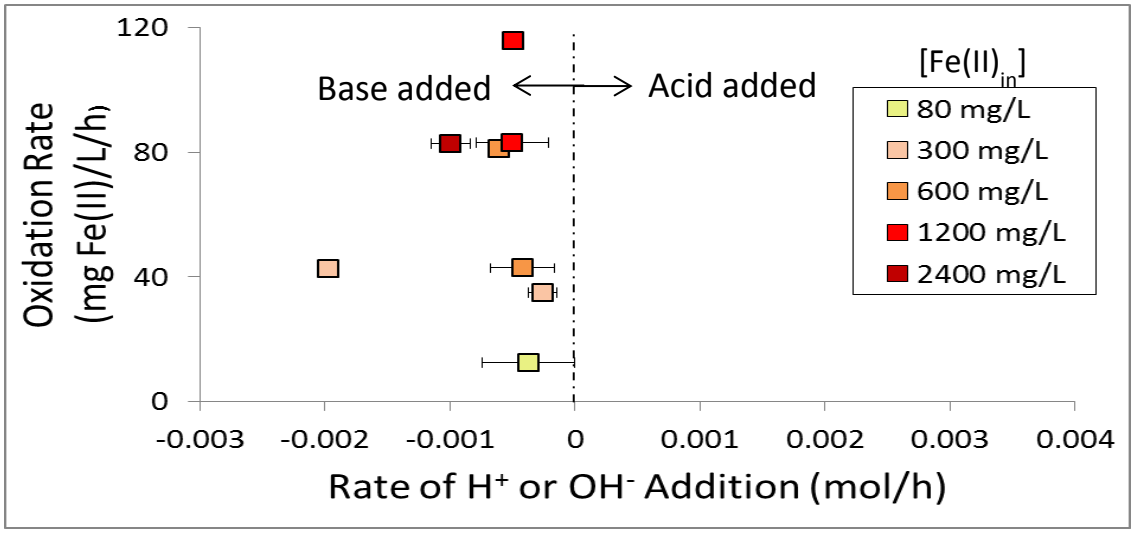

Figure 4-9: Only base was added to maintain the pH during the varying influent Fe(II) concentration experiment. This is evidence that both Fe(II) oxidation and Fe(III) precipitation occurred in the bioreactor.

The previous two plots show evidence that certain reactions are occurring at different operating conditions. In Figure 4-8, acid addition when the reactor pH < 2.9 shows evidence that mainly Fe(II) oxidation was occurring (Reaction 2), and base addition when the reactor pH > 2.9 shows evidence that both Fe(II) oxidation and Fe(III) precipitation are occurring (Reactions 2 and 4). Two points were measured at pH=2.9, with one requiring base addition and the other requiring acid addition. In Figure 4-9, the data for the varying influent Fe(II) concentration experiment, which was run at pH=2.9, show that base was required for the entire experiment. For the varying hydraulic residence time tests that were run at pH=2.9, acid was required for both experiments. Therefore, pH=2.9 needs to be explored more because the data do not show evidence for the occurrence of only oxidation or both oxidation and precipitation.

Knowing whether Fe(II) oxidation is the dominant reaction is important for reactor design. For example, if a treatment system has separate reactors for Fe(II) oxidation and Fe(III) precipitation, then operating the oxidation reactor at pH=4.1 will cause undesirable precipitation to occur within that reactor. However, both oxidation and precipitation may actually be preferred, and so special attention needs to be paid to the reactor's pH.

Total Iron Removal Rate Estimates

An important aspect of the reactor design is the amount of the total iron that is removed from the AMD per day. Different operating conditions yield higher removal rates than others. The daily load-based removal per area of total iron can be calculated using Equation 4-6,

$$\mathrm{GDM} = \left(\frac{([\mathrm{Fe(T)_{in}}] - [\mathrm{Fe(T)_{out}}])\mathrm{Q}}{\mathrm{A}}\right) \qquad (\mathrm{Eq.}\ 4-6)$$

where, GDM is the daily load of iron removed in (g Fe(T)/d/m^2), Q is the flow rate in (L/h), and A is the area of the reactor in plan-view in (m^2). The plots of GDM as a function of the reactor pH and influent Fe(II) concentration are shown in Figures 4-10 and 4-11. The influent Fe(II) concentration was used instead of the effluent concentration in Figure 4-11 because the design of a reactor will be based on the natural concentration in the AMD (the influent concentration) at the site.

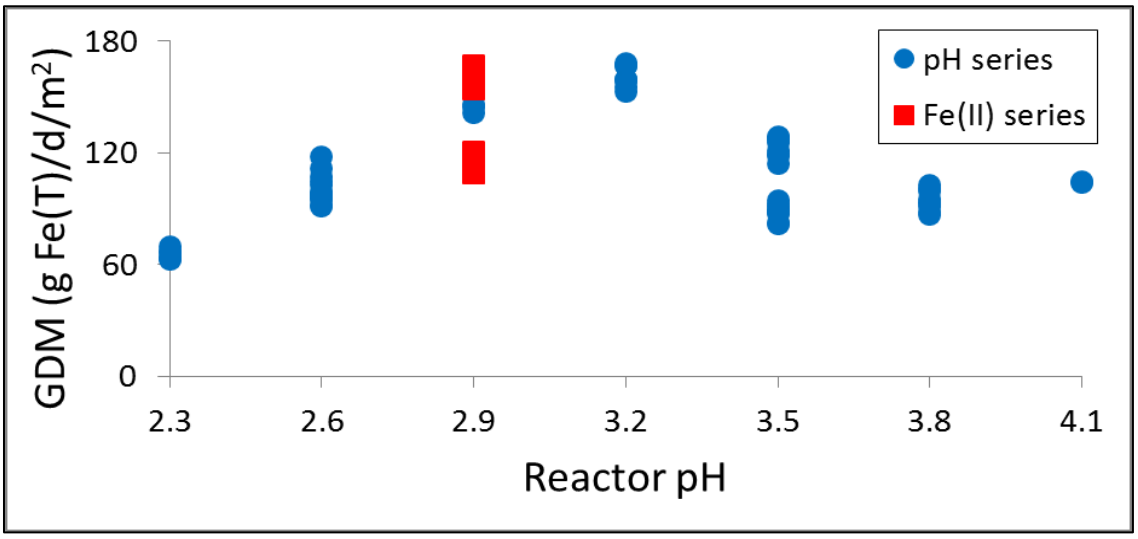

Figure 4-10: The GDM values increase and appear to reach a maximum around a pH of about 2.9 and 3.2.

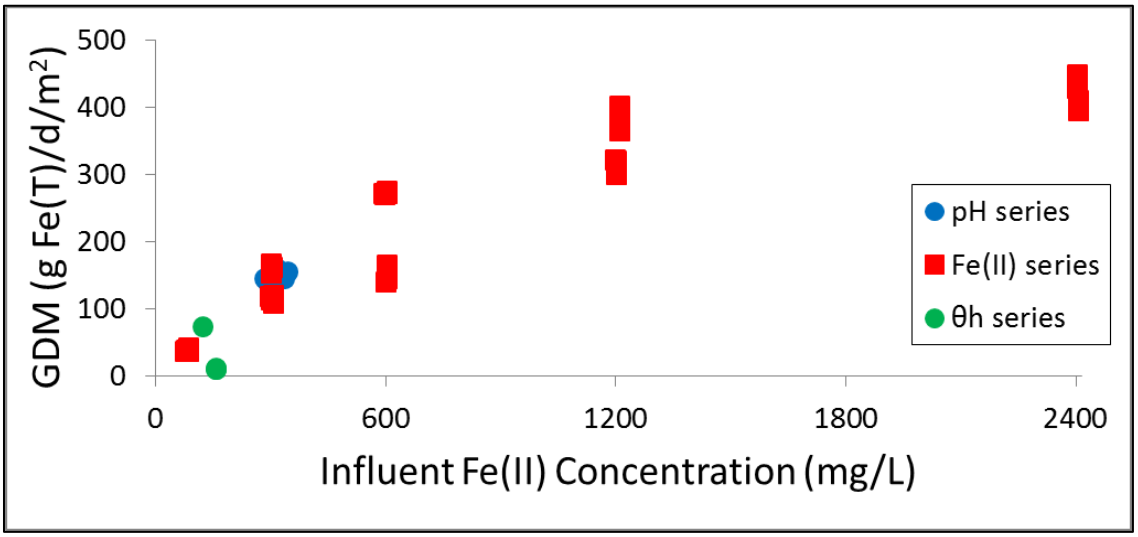

Figure 4-11: The GDM values increase and appear to reach a maximum as the influent Fe(II) concentration increases.

Reported GDM values in the literature are much less than the ones measured in the bioreactor. The range of 2.6-8.7 GDM was found for laboratory tests using sediment from seven AMD sites in Pennsylvania and West Virginia, and these values are consistent with other reported values.[16] Since the GDM values are much greater for the bioreactor used in this work, it should be considered a viable option for removing total iron from AMD. The amount of land required for a reactor with a very high GDM is much less than that of a settling pond or wetland with a lower GDM. The GDM for the reactor could even possibly be increased by making the reactor deeper while keeping the plan-view area the same.

Conclusions and Future Work

This research has provided insights into the treatment of iron in low-pH AMD from coalmines. The oxidation of Fe(II) occurs naturally at many AMD sites, and this work aimed at utilizing this natural treatment process in an engineered bioreactor. The following conclusions can be drawn from this study.

1. Enriching a mixed culture of organisms from sediment and water collected from an AMD site proved to be feasible. Two enrichment cultures were grown in batch mode from freshly collected site samples. These enrichment cultures produced viable bioreactors that were used for flow-through experiments. There is no indication that these enrichment cultures could not be scaled up to larger reactors.
2. The hydraulic residence time of 6 h was found to be optimal for this system. Increasing θ_h produced only slightly higher oxidation efficiencies, while decreasing it caused much lower efficiencies.
3. The rates of Fe(II) oxidation increased with a decreasing reactor pH and with an increasing influent Fe(II) concentration. A saturation-like effect appeared to occur with increasing influent Fe(II) concentrations, and also possibly with decreasing pH, although more data is needed to verify this.
4. The biomass concentration appeared to be remarkably stable throughout the course of the experiments. The majority of the biomass was found to be present in the biofilm, and only a small fraction was in suspension. There appeared to be no correlation between the oxidation rates and biomass concentrations in these experiments
5. A general rate law for the Fe(II) oxidation rate was found to be a function of the hydrogen ion concentration and influent Fe(II) concentration. The data for both of these variables were fit with Monod curves, and then these Monod expressions were substituted into the general rate law equation. The rate law equation was used as a model to predict oxidation rates for the completed experiments, but the model showed deficiencies. More data and possibly more terms in the rate law equation should be used to further refine the model and produce more accurate results.
6. Based on additions of acid and base during the experiments, the data showed evidence that at pH < 2.9 there was evidence of primarily Fe(II) oxidation occurring, while at

pH > 2.9 there was evidence of both oxidation and precipitation occurring. pH=2.9 needs to be explored more because the data do not show evidence for the occurrence of only oxidation or both oxidation and precipitation.

7. The loading rates per area for the bioreactor were much higher than those reported in the literature. Depending on the operating condition, the bioreactor achieved GDM values over the range of 9-448 g Fe(T)/d/m^2, with many of them being greater than 100 g Fe(T)/d/m^2. This means the bioreactor can remove much more total iron per square area than other treatment techniques; therefore, it should be considered a viable option for the removal of total iron from AMD.

This work has answered questions about the operating parameters of a bioreactor treating low-pH AMD from a coalmine, but before implementing this type of reactor for treatment at a site, more work needs to be done. First, running the exact same experiments using sediment and water form a different AMD site would provide valuable information that tells if these rates are site specific or applicable to multiple sites. Other key experiments would test the effects of temperature, agitation (from both stirring and air sparging), sulfate concentration, and other metal concentrations (aluminum, manganese, etc.) on Fe(II) oxidation rates. Finally, the sequencing of the microbes present in the bioreactors could provide important insights into the microbial community structure for different operating conditions. All of this work, both present and future, will hopefully contribute to help making bioreactors a more feasible option for AMD treatment.

References

1. Brown, J.F., Jones, D.S., Mills, D.B., Macalady, J.L., Burgos, W.D. 2011. Application of a Depositional Facies Model to an Acid Mine Drainage Site. Appl. Environ. Microbiol. 77:545-554.
2. Chen, C.J., Jiang, W.T. 2012. Influence of waterfall aeration and seasonal temperature variation on the iron and arsenic attenuation rates in an acid mine drainage system. Appl. Geochem. 27:1966-1978.
3. Clearfield Creek Watershed Association. 2003. Brubaker Run Acid Drainage Remediation. Accessed 10/31/13. <http://www.clearfieldcreekwatershed.org/projects/brubaker.html>.
4. Cole, M., Wrubel, J., Henegan, P., Janzen, C., Holt, J., Tobin, T. 2011. Development of a small-scale bioreactor method to monitor the molecular diversity and environmental impacts of bacterial biofilm communities from an acid mine drainage impacted creek. J. Microbiol. Meth. 87:96-104.
5. Cravotta III, C.A. 2008. Dissolved metals and associated constituents in abandoned coal-mine discharges, Pennsylvania, USA. Part 1: Constituent quantities and correlations. Appl. Geochem. 23:166-202.
6. Diz, H.R. 1997. Chemical and Biological Treatment of Acid Mine Drainage for the Removal of Heavy Metals and Acidity. Ph.D. dissertation, Virginia Polytechnic Institute and State University.
7. Ford, K.L. 2003. Passive treatment systems for acid mine drainage. Technical Note 409. BLM/ST/St-002/001+3596. Bureau of Land Management.
8. Hedrich, S., Johnson, D.B. 2012. A modular continuous flow reactor system for the selective bio-oxidation of iron and precipitation of schwertmannite from mine-impacted waters. Bioresour. Technol. 106:44-49.
9. Ishii, S., Watanabe, K., Yabuki, S., Logan, B.E., Sekiguchi, Y. 2008. Comparison of Electrode Reduction Activities of *Geobacter sulfurreducens* and an Enriched Consortium in an Air-Cathode Microbial Fuel Cell. Appl. Environ. Microbiol. 74:7348-7355.
10. Janneck, E., Arnold, I., Koch, T., Meyer, J., Burghardt, D., Ehinger, S. 2010. Microbial synthesis of schwertmannite from lignite mine water and its utilization for removal of arsenic from mine waters and for production of iron pigments. Mine Water and Innovative Thinking, IMWA. 131-134.
11. Johnson, D. B. 2003. Chemical and Microbiological Characteristics of Mineral Spoils and Drainage Waters at Abandoned Coal and Metal Mines. Water, Air, Soil Pollut. 3:47-66.
12. Johnson, D.B., Hallberg, K.B. 2004. Acid mine drainage remediation options: a review. Sci. Total Environ. 338:3-14.
13. Karamanev, D.G., Nikolov, L.N. 1988. Influence of Some Physicochemical Parameters on Bacterial Activity of Biofilm: Ferrous Iron Oxidation by Thiobacillus ferrooxidans. Biotechnol. Bioeng. 31:295-299.
14. Kirby, C.S., Brady, J.A.E. 1998. Field determination of Fe^{2+} oxidation rates in acid mine drainage using a continuously-stirred tank reactor. Appl. Geochem. 13:509-520.
15. Kirby, C.S., Thomas, H.M., Southam, G., Donald, R. 1999. Relative contributions of abiotic and biological factors in Fe(II) oxidation in mine drainage. Appl. Geochem. 14:511-530.
16. Larson, L.N., Sánchez España, J., Burgos, W.D. Submitted September 2013. Rates of low pH biological Fe(II) oxidation in the Appalachian Bituminous Coal Basin and the Iberian Pyrite Belt. Appl. Geochem.
17. Lovely, D.R., Phillips, E.J.P. 1987. Rapid Assay for Microbially Reducible Ferric Iron in Aquatic Sediments. Appl. Environ. Microbiol. 53:1536-1540.

18. Nakamura, K., Noike, T.; Matsumoto, J. 1986. Effect of operation conditions on biological Fe^{2+} oxidation with rotating biological contactors. Wat. Res. 20:73-77.
19. Ňancucheo, I., Hedrich, S., Johnson, D.B. 2012. New microbiological strategies that enable the selective recovery and recycling of metals from acid mine drainage and mine process waters. Mineral Mag. 76:2683-2692.
20. Nikolov, L.N., Karamanev, D.G. 1990. The Inverse Fluidized Bed Biofilm Reactor: A New Laboratory Scale Apparatus for Biofilm Research. J. Ferment. Bioeng. 69:265-267.
21. Nordstrom, D.K. 2000. Advances in the Hydrogeochemistry and Microbiology of Acid Mine Waters. International Geology Review. 42:499-515.
22. Nordstrom, D.K. 2011. Mine Waters: Acidic to Circumneutral. Elements. 7:393-398.
23. Pesic, B., Oliver, D.J., Wichlacz, P. 1989. An Electrochemical Method of Measuring the Oxidation Rate of Ferrous to Ferric Iron with Oxygen in the Presence of *Thiobacillus ferrooxidans*. Biotechnol. Bioeng. 33:428-439.
24. Oz, N.A., Ince, O., Ince, B.K., Akarsubasi, A.T., Eyice, O. 2007. Microbial Population Dynamics in an Anaerobic CSTR Treating a Chemical Synthesis-Based Pharmaceutical Wastewater. J. Environ. Sci. Health., Part A. A38:2029-2042.
25. Ramsay, B., Ramsay, J., de Tremblay, M., Chavarie, C. 1988. A Method for the Quantification of Bacterial Protein in the Presence of Jarosite. Geomicrobiol. J. 6:171-177.
26. Rose, A.W., Cravotta III, C.A. 1998. Geochemistry of Coal Mine Drainage. In: Coal Mine Drainage Prediction and Pollution Prevention in Pennsylvania. Pennsylvania Department of Environmental Protection. 1.1-1.22.
27. Sánchez España, J., López Pamo, E., Santofimia Pastor, E. 2007. The oxidation of ferrous iron in acidic mine effluents from the Iberian Pyrite Belt (Odiel Basin, Huelva, Spain): Field and laboratory rates. J. Geochem. Explor. 92:120-132.
28. Shuler, M.L, Kargi, F. 2001. Bioprocess Engineering. 2nd ed. Prentice Hall, Upper Saddle River, NJ.
29. Stumm, W., Lee, F.G. 1961. Oxygenation of Ferrous Iron. Ind. Eng. Chem. 53:143-146.
30. Taylor, W., Dunn, M., Busler, S. 2003. Chapter 4: Naturally Innovative Solutions. In: Accepting the Challenge. 2nd ed. Slippery Rock Watershed Coalition. 50.

Appendix

Raw Data

Table A-1. The raw data is shown for the steady-state points, with respect to Fe(II) oxidation, of the first varying hydraulic residence time test.

Θ_h (h)	Influent dissolved [Fe(II)] (mg/L)	Reactor pH	Reactor DO (mg/L)	Effluent dissolved [Fe(II)] (mg/L)	Effluent dissolved [Fe(III)] (mg/L)	Titrant added (NaOH or H_2SO_4)	Titrant addition rate (mol H^+ or OH^-/h)	T (°C)	$C_{bacteria}$ (cells/mL)
24	148.7	2.9	3.80	1.5	83.0	H_2SO_4	2.22E-04	20	
12	158.9	2.9	3.35	2.4	88.5	H_2SO_4	2.32E-04	20	
12	158.9	2.9	3.74	2.2	90.4	H_2SO_4	2.84E-04	20	
12	158.9	2.9	3.54	2.1	98.2	H_2SO_4	3.51E-04		
12	158.9	2.9	3.47	2.2	90.9	H_2SO_4	3.45E-04	20	
6	158.9	2.9	3.32	4.0	91.5	H_2SO_4	3.43E-04	20	
6	158.9	2.9	3.08	4.4	98.1	H_2SO_4	3.44E-04	20	
6	158.9	2.9	3.06	4.4	106.8	H_2SO_4	3.20E-04	20	
6	158.9	2.9	3.76	4.3	98.6	H_2SO_4	2.86E-04	20	
6	158.9	2.9	2.95	4.2	110.2	H_2SO_4	5.32E-04	20	
3	92.9	2.9	2.93	4.5	98.7	H_2SO_4	5.49E-04	20	
3	63.2	2.9	3.02	3.1	72.6	H_2SO_4	5.50E-04	20	
3	63.2	2.9	2.95	3.1	72.7	H_2SO_4	5.72E-04	20	
3	63.2	2.9	2.85	3.2	69.7	H_2SO_4	5.35E-04	20	
1	151.0	2.9	2.77	31.1	76.9	H_2SO_4	5.48E-04	20	
1	151.0	2.9	2.74	30.5	73.4	H_2SO_4	5.34E-04	20	
1	151.0	2.9	2.72	31.5	74.2	H_2SO_4	5.54E-04	20	
1	151.0	2.9	2.70	31.1	75.8	H_2SO_4	5.39E-04	20	
0.75	151.0	2.9	2.65	39.2	71.8	H_2SO_4	5.35E-04	20	
0.75	151.0	2.9	2.67	39.6	63.3	H_2SO_4	5.38E-04	20	
0.75	151.0	2.9	2.66	41.1	74.0	H_2SO_4	5.26E-04	20	
0.75	151.0	2.9	2.64	42.1	65.2	H_2SO_4	5.45E-04	20	
0.75	151.0	2.9	2.72	40.9	64.3	H_2SO_4	5.63E-04	20	
0.75	151.0	2.9	2.65	41.3	73.7	H_2SO_4	4.80E-05	20	
0.75	151.0	2.9	2.61	40.7	70.0	H_2SO_4	1.09E-04	20	
0.5	147.0	2.9	2.51	49.1	63.6	H_2SO_4	7.75E-04	20	
0.5	147.0	2.9	2.58	49.2	67.3	H_2SO_4	5.90E-04	20	
0.5	147.0	2.9	2.56	49.2	57.2	H_2SO_4	7.80E-04	20	
0.5	147.0	2.9	2.55	49.2	60.6	H_2SO_4	8.15E-04	20	
0.5	147.0	2.9	2.54	49.0	54.5	H_2SO_4	7.90E-04	20	
3	139.6	2.9	3.13	3.8	66.3	H_2SO_4	2.45E-04	20	
3	139.6	2.9	2.58	3.6	75.8	H_2SO_4	3.19E-04	20	
6	134.0	2.9	2.29	0.7	72.9	H_2SO_4	9.36E-04	20	

Table A-2. The raw data is shown for the steady-state points, with respect to Fe(II) oxidation, of the second varying hydraulic residence time test.

Θ_h (h)	Influent dissolved [Fe(II)] (mg/L)	Reactor pH	Reactor DO (mg/L)	Effluent dissolved [Fe(II)] (mg/L)	Effluent dissolved [Fe(III)] (mg/L)	Titrant added (NaOH or H_2SO_4)	Titrant addition rate (mol H^+ or OH^-/h)	T (°C)	$C_{bacteria}$ (cells/mL)
24	129.40	2.9	5.60	3.07	44.23	H_2SO_4	3.72E-04	20	
24	115.80	2.9	5.41	2.70	35.10	H_2SO_4	3.22E-04	20	
12	164.10	2.9	5.20	4.90	50.20	H_2SO_4	1.74E-04	20	
12	164.10	2.9	5.29	5.00	48.90	H_2SO_4	0.00E+00	20	
6	142.45	2.9	5.02	8.45	46.30	H_2SO_4	8.62E-04	20	
6	127.35	2.9	5.02	7.80	42.75	H_2SO_4	5.59E-04	20	
6	127.60	2.9	5.22	7.75	50.55	H_2SO_4	1.73E-05	20	
6	124.25	2.9	5.03	7.53	43.53	H_2SO_4	3.61E-04	20	
3	180.15	2.9	4.61	46.65	46.65	H_2SO_4	8.48E-04	20	
3	180.45	2.9	4.59	46.70	45.70	H_2SO_4	5.79E-04	20	
3	180.50	2.9	4.53	47.90	47.10	H_2SO_4	4.87E-04	20	
3	181.10	2.9	4.49	47.40	49.75	H_2SO_4	3.98E-04	20	
1	157.75	2.9	5.28	67.30	32.80	H_2SO_4	3.20E-03	20	
1	165.35	2.9	5.26	73.35	26.60	H_2SO_4	3.01E-03	20	
1	161.80	2.9	5.25	72.20	32.50	H_2SO_4	3.00E-03	20	
1	160.15	2.9	5.24	71.45	34.50	H_2SO_4	3.04E-03	20	
0.75	140.70	2.9	5.17	79.30	12.65	H_2SO_4	4.21E-03	20	
0.75	129.85	2.9	5.15	76.70	4.40	H_2SO_4	4.28E-03	20	
0.75	124.30	2.9	5.19	73.75	12.10	H_2SO_4	4.12E-03	20	
0.75	122.65	2.9	5.18	71.40	15.25	H_2SO_4	4.08E-03	20	
0.75	120.85	2.9	5.18	70.65	15.55	H_2SO_4	4.12E-03	20	
0.75	120.40	2.9	5.12	70.00	17.70	H_2SO_4	4.12E-03	20	
0.5	157.34	2.9	4.77	93.99	23.46	H_2SO_4	1.59E-02	20	
0.5	158.95	2.9	4.75	94.40	26.65	H_2SO_4	1.52E-02	20	
0.5	156.30	2.9	4.95	93.81	17.26	H_2SO_4	1.48E-02	20	
1	146.47	2.9	4.88	65.80	55.95	H_2SO_4	1.78E-03	20	
1	147.07	2.9	4.89	64.43	46.36	H_2SO_4	1.19E-03	20	
1	146.12	2.9	4.81	61.40	54.34	H_2SO_4	5.07E-03	20	
1	145.81	2.9	4.81	63.76	54.17	H_2SO_4	4.56E-03	20	
3	166.85	2.9	4.82	35.76	73.01	H_2SO_4	0.00E+00	20	
3	167.17	2.9	4.83	36.37	71.58	H_2SO_4	0.00E+00	20	

Table A-3. The raw data is shown for the steady-state points, with respect to Fe(II) oxidation, of the varying reactor pH test.

Θ_h (h)	Influent dissolved [Fe(II)] (mg/L)	Reactor pH	Reactor DO (mg/L)	Effluent dissolved [Fe(II)] (mg/L)	Effluent dissolved [Fe(III)] (mg/L)	Titrant added (NaOH or H_2SO_4)	Titrant addition rate (mol H^+ or OH^-/h)	T (°C)	$C_{bacteria}$ (cells/mL)
6	355.64	2.9	7.93	55.62	63.56	H_2SO_4	4.25E-05	20	
6	337.10	2.9	6.25	53.98	39.09	H_2SO_4	2.56E-04	20	
6	343.53	2.9	6.25	54.86	54.10	H_2SO_4	4.20E-04	20	
6	345.80	2.9	8.32	56.37	43.51	H_2SO_4	8.99E-04	20	6.30E+06
6	306.89	2.6	5.08	33.33	141.53	H_2SO_4	9.71E-04	20	
6	301.54	2.6	4.91	33.07	165.22	H_2SO_4	1.16E-03	20	
6	329.15	2.6	5.55	36.09	144.79	H_2SO_4	5.71E-04	20	1.88E+07
6	312.39	2.3	4.89	17.33	162.61	H_2SO_4	3.16E-03	20	
6	306.74	2.3	4.83	17.79	172.17	H_2SO_4	3.32E-03	20	
6	289.81	2.3	5.34	15.78	161.17	H_2SO_4	3.25E-03	20	
6	331.05	2.3	7.42	18.27	179.06	H_2SO_4	2.74E-03	20	
6	314.02	2.3	7.24	17.75	159.37	H_2SO_4	2.45E-03	20	9.40E+06
6	304.41	2.6	8.59	10.46	148.42	H_2SO_4	5.48E-04	20	7.70E+06
6	284.13	2.9	5.90	32.72	48.32	NaOH	1.01E-03	20	
6	314.23	2.9	6.33	36.61	55.19	NaOH	7.79E-04	20	2.27E+07
6	309.22	3.2	7.06	73.02	8.54	NaOH	7.57E-04	20	
6	303.68	3.2	7.12	73.27	6.94	NaOH	1.09E-03	20	
6	296.93	3.2	6.62	70.19	16.42	NaOH	1.75E-03	20	
6	299.72	3.2	6.59	73.29	7.95	NaOH	1.07E-03	20	
6	307.76	3.2	6.36	76.42	6.54	NaOH	1.61E-03	20	
6	302.99	3.2	5.75	73.63	4.33	NaOH	1.13E-03	20	
6	314.12	3.2	5.51	78.21	4.25	NaOH	1.87E-03	20	
6	307.13	3.2	5.89	74.10	10.22	NaOH	5.14E-04	20	1.05E+07
6	308.21	3.5	5.11	120.47	37.75	NaOH	4.43E-04	20	
6	301.75	3.5	4.80	118.04	40.46	NaOH	4.24E-04	20	
6	307.29	3.5	4.46	125.16	15.99	NaOH	5.73E-04	20	4.67E+06
6	302.40	3.8	4.52	104.05	12.39	NaOH	1.66E-03	20	
6	298.84	3.8	4.36	99.10	39.58	NaOH	1.53E-03	20	
6	299.08	3.8	4.08	98.53	24.31	NaOH	1.69E-03	20	
6	297.16	3.8	3.81	100.04	14.17	NaOH	1.56E-03	20	
6	303.07	3.8	3.74	104.62	11.65	NaOH	1.63E-03	20	1.22E+07
6	297.46	4.1	3.52	123.04	43.89	NaOH	1.83E-03	20	
6	296.71	4.1	3.33	123.54	48.19	NaOH	1.86E-03	20	
6	301.30	4.1	7.39	121.51	6.75	NaOH	3.07E-02	20	
6	307.29	4.1	7.62	117.98	6.61	NaOH	3.03E-03	20	
6	303.50	4.1	5.21	122.54	4.03	NaOH	2.21E-03	20	9.15E+06
6	303.81	3.8	5.09	153.86	25.34	NaOH	1.15E-03	20	
6	303.81	3.8	4.15	153.40	13.38	NaOH	1.59E-03	20	
6	303.81	3.8	3.76	150.14	25.14	NaOH	1.55E-03	20	
6	303.81	3.8	3.46	147.28	22.98	NaOH	1.28E-03	20	
6	303.81	3.8	3.23	146.69	32.17	NaOH	1.23E-03	20	4.80E+06
6	301.88	3.5	4.12	171.22	43.97	NaOH	1.60E-05	20	
6	302.20	3.5	3.72	180.83	41.16	NaOH	1.15E-03	20	
6	305.32	3.5	3.13	177.06	29.51	NaOH	1.08E-03	20	
6	306.12	3.5	2.83	173.93	33.61	NaOH	1.08E-03	20	
6	298.05	3.5	2.53	172.73	29.84	NaOH	1.01E-03	20	
6	302.91	3.5	2.38	178.30	30.86	NaOH	9.64E-04	20	4.45E+06

Table A-4. The raw data is shown for the steady-state points, with respect to Fe(II) oxidation, of the varying influent Fe(II) concentration test.

Θ_h (h)	Influent dissolved [Fe(II)] (mg/L)	Reactor pH	Reactor DO (mg/L)	Effluent dissolved [Fe(II)] (mg/L)	Effluent dissolved [Fe(III)] (mg/L)	Titrant added (NaOH or H_2SO_4)	Titrant addition rate (mol H^+ or OH^-/h)	T (°C)	$C_{bacteria}$ (cells/mL)
6	306.76	2.9	8.03	94.66	63.10	NaOH	4.22E-04	20	
6	303.44	2.9	7.58	91.98	68.33	NaOH	3.77E-04	20	
6	310.03	2.9	7.43	95.30	69.45	NaOH	3.14E-04	20	
6	307.70	2.9	7.46	99.00	66.74	NaOH	2.68E-04	20	
6	307.19	2.9	7.31	98.20	59.79	NaOH	2.17E-04	20	
6	301.84	2.9	7.19	93.90	74.09	NaOH	2.09E-04	20	
6	298.79	2.9	6.85	93.05	75.21	NaOH	1.72E-04	20	
6	303.32	2.9	6.84	96.60	76.79	NaOH	6.71E-05	20	2.99E+07
6	88.31	2.9	6.56	8.86	29.41	NaOH	1.12E-04	20	
6	78.33	2.9	6.51	8.20	26.47	NaOH	6.36E-04	20	9.10E+06
6	305.12	2.9	6.09	48.83	5.35	NaOH	1.97E-03	20	
6	296.97	2.9	6.43	45.32	8.92	NaOH	*	20	
6	300.01	2.9	6.36	48.55	2.62	NaOH	*	20	
6	301.50	2.9	6.63	47.65	2.11	NaOH	*	20	1.72E+07
6	598.15	2.9	7.75	112.97	35.85	NaOH	0.00E+00	20	
6	595.75	2.9	7.52	112.78	14.06	NaOH	1.13E-03	20	
6	601.16	2.9	7.39	113.56	12.02	NaOH	7.17E-04	20	
6	603.11	2.9	6.74	115.01	9.42	NaOH	5.99E-04	20	1.55E+07
6	1208.78	2.9	5.75	526.43	55.28	NaOH	3.67E-04	20	
6	1208.78	2.9	5.52	498.10	105.34	NaOH	5.36E-04	20	
6	1208.78	2.9	5.38	520.92	96.04	NaOH	5.63E-04	20	
6	1208.78	2.9	5.23	513.39	98.06	NaOH	5.13E-04	20	6.20E+06
6	2409.03	2.9	5.18	1915.48	38.60	NaOH	8.84E-04	20	
6	2411.48	2.9	5.03	1894.29	15.37	NaOH	*	20	
6	2393.22	2.9	5.01	1893.55	62.78	NaOH	1.10E-03	20	
6	2405.08	2.9	4.47	1855.32	66.63	NaOH	*	20	
6	2403.10	2.9	4.41	1845.34	46.98	NaOH	*	20	
6	2405.07	2.9	4.26	1865.49	46.75	NaOH	*	20	2.43E+06
6	1206.33	2.9	4.20	721.93	32.46	NaOH	4.44E-04	20	
6	1197.82	2.9	4.23	701.23	23.19	NaOH	6.91E-04	20	
6	1202.50	2.9	1.49	689.12	45.03	NaOH	1.19E-04	20	
6	1202.47	2.9	2.36	704.90	66.54	NaOH	7.44E-04	20	2.64E+06
6	604.36	2.9	4.01	174.16	23.19	NaOH	6.02E-04	20	
6	599.76	2.9	7.09	173.91	20.73	NaOH	2.41E-04	20	5.25E+06

*titrant addition rate omitted because the chemostat severely overestimated the amount of titrant added during this interval

Table A-4. Measurements of the reactor's geometry are shown. The flow conditions are also shown for the operating condition of Θ_h=6 h.

$D_{reactor}$=	12.5	cm
$A_{reactor}$=	0.0123	m^2
Q=	0.3333	L/h
Q=	8	L/d
Θ_h=	6	h

Table A-5. The raw data is shown for the steady-state points, with respect to Fe(T) removal, of the first varying hydraulic residence time test.

Θ_h (h)	Influent total [Fe(T)] (mg/L)	Reactor pH	Effluent total [Fe(T)] (mg/L)
24	156.5	2.9	92.8
24	156.5	2.9	97.2
24	156.5	2.9	91.3
24	156.5	2.9	90.3
12	178.8	2.9	96.7
12	178.8	2.9	97.7
12	178.8	2.9	94.2
6	178.8	2.9	109.5
6	178.8	2.9	113.1
6	178.9	2.9	119.4
3	113.8	2.9	77.1
3	113.8	2.9	77.4
3	113.8	2.9	76.5
1	173.7	2.9	106.6
1	173.7	2.9	108.4
1	173.7	2.9	109.3
1	173.7	2.9	104.2
1	173.7	2.9	106.9
1	173.7	2.9	109
0.75	173.7	2.9	112
0.75	173.7	2.9	114.1
0.75	173.7	2.9	115.5
0.75	173.7	2.9	108.3
0.75	173.7	2.9	108.3
0.75	173.7	2.9	116.3
0.75	173.7	2.9	118.5
0.5	179	2.9	126.3
0.5	179	2.9	118.2
0.5	179	2.9	117.9
0.5	179	2.9	114.8
0.5	179	2.9	112.04
0.5	179	2.9	112.04
3	177.1	2.9	86.5
3	177.1	2.9	86.8
6	173.7	2.9	78
6	173.7	2.9	77
6	173.7	2.9	80.4

Table A-6. The raw data is shown for the steady-state points, with respect to Fe(T) removal, of the second varying hydraulic residence time test.

Θ_h (h)	Influent total [Fe(T)] (mg/L)	Reactor pH	Effluent total [Fe(T)] (mg/L)
24	153.3	2.9	65.7
24	116.9	2.9	49.9
12	175.6	2.9	61.3
12	181.3	2.9	63.6
12	181.3	2.9	62.1
6	167.85	2.9	53.8
3	201.3	2.9	109.8
3	198.9	2.9	109.2
3	199.05	2.9	108.4
3	200.85	2.9	106.85
1	158.9	2.9	109.6
1	174.15	2.9	126.2
1	179.45	2.9	130.1
0.75	144.95	2.9	120.9
0.75	147.15	2.9	115.4
0.75	145.55	2.9	115.35
0.75	144.65	2.9	116.4
0.5	180.425	2.9	136.16
0.5	180.4	2.9	135.75
0.5	177.92	2.9	135.8
0.5	181.84	2.9	132.76
1	181.405	2.9	144.53
1	183.83	2.9	140.1
3	207.71	2.9	129.395
3	194.725	2.9	124.79

Table A-7. The raw data is shown for the steady-state points, with respect to Fe(T) removal, of the varying reactor pH test.

Θ_h (h)	Influent total [Fe(T)] (mg/L)	Reactor pH	Effluent total [Fe(T)] (mg/L)
6	352.99	2.9	129.0
6	370.01	2.9	131.7
6	334.50	2.6	194.1
6	343.60	2.6	191.9
6	335.03	2.6	193.9
6	400.00	2.6	218.6
6	374.55	2.6	210.5
6	344.48	2.3	247.7
6	340.79	2.3	243.0
6	350.91	2.3	254.9
6	341.42	2.3	238.6
6	374.55	2.3	267.8
6	342.77	2.3	241.1
6	342.91	2.6	196.5
6	355.75	2.6	205.3
6	352.68	2.6	202.6
6	340.50	2.6	193.3
6	340.52	2.6	194.1
6	350.72	2.6	193.5
6	349.58	2.6	201.2
6	370.08	5.6	199.3
6	359.72	2.6	199.2
6	342.14	2.9	104.3
6	318.94	2.9	97.4
6	310.99	2.9	94.0
6	359.80	2.9	113.6
6	363.70	3.2	119.3
6	372.80	3.2	116.4
6	358.60	3.2	114.5
6	359.26	3.2	120.6
6	366.93	3.2	122.6
6	379.59	3.2	123.7
6	352.68	3.2	118.3
6	380.09	3.2	121.9
6	349.17	3.5	163.7
6	386.84	3.5	192.5
6	384.74	3.5	188.4
6	364.78	3.5	181.6
6	374.34	3.5	181.7
6	371.34	3.5	173.7
6	356.50	3.5	181.2
6	354.74	3.5	173.2
6	360.93	3.8	217.9
6	357.82	3.8	222.6
6	358.38	3.8	212.1
6	360.44	3.8	220.5
6	349.20	3.8	216.3
6	360.10	3.8	217.5
6	351.85	4.1	192.2
6	363.17	4.1	202.8
6	368.49	3.8	215.6
6	368.49	3.8	211.0
6	368.49	3.8	213.5
6	363.41	3.5	227.2
6	354.58	3.5	219.9
6	371.24	3.5	229.2
6	364.79	3.5	227.8
6	362.07	3.5	235.2
6	368.88	3.5	228.9
6	374.06	3.5	229.2
6	357.06	3.5	231.9
6	361.30	3.5	226.3

Table A-8. The raw data is shown for the steady-state points, with respect to Fe(T) removal, of the varying influent Fe(II) concentration test.

Θ_h (h)	Influent total [Fe(T)] (mg/L)	Reactor pH	Effluent total [Fe(T)] (mg/L)	Influent dissolved [Fe(II)] set point (mg/L)
6	366.61	2.9	181.6	300
6	364.34	2.9	197.0	300
6	361.24	2.9	192.8	300
6	364.30	2.9	189.3	300
6	375.45	2.9	194.0	300
6	380.23	2.9	198.1	300
6	97.84	2.9	37.5	80
6	104.89	2.9	41.2	80
6	100.38	2.9	40.6	80
6	95.44	2.9	38.6	80
6	95.28	2.9	37.7	80
6	361.49	2.9	112.8	300
6	390.56	2.9	134.2	300
6	352.23	2.9	115.6	300
6	646.31	2.9	233.1	600
6	645.70	2.9	229.7	600
6	645.07	2.9	222.3	600
6	636.45	2.9	219.2	600
6	646.65	2.9	229.1	600
6	1348.90	2.9	789.9	1200
6	1348.90	2.9	755.8	1200
6	1348.90	2.9	733.8	1200
6	1348.90	2.9	745.1	1200
6	1348.90	2.9	762.6	1200
6	2576.45	2.9	1969.8	2400
6	2599.05	2.9	1971.1	2400
6	2591.15	2.9	1933.8	2400
6	2600.50	2.9	1913.2	2400
6	1366.90	2.9	873.3	1200
6	1353.50	2.9	862.9	1200
6	1340.93	2.9	881.0	1200
6	694.87	2.9	315.4	600
6	672.29	2.9	299.6	600
6	666.13	2.9	306.8	600